

Alzheimer's disease-related presenilins are key to intestinal epithelial cell function and gut immune homeostasis

Lena Erkert¹, Reyes Gamez Belmonte¹, Melanie Kabisch¹, Lena Schödel¹, Jay V. Patankar^{1 2}, Miguel Gonzalez Acera¹, Mousumi Mahapatro¹, Li-Li Bao¹, Christina Plattner³, Anja A. Kühl⁴, Jie Shen⁵, Lutgarde Serneels⁶, Bart De Strooper^{6 7}, TRR241 IBDome Consortium, Markus F. Neurath^{1 2}, Stefan Wirtz^{1 2} and Christoph Becker^{1 2*}

¹ Department of Medicine 1, Universitätsklinikum Erlangen, Friedrich-Alexander-Universität Erlangen-Nürnberg, Germany.

² Deutsches Zentrum Immuntherapie (DZI), Erlangen, Germany.

³ Institute for Bioinformatics, Medical University of Innsbruck, Innsbruck, Austria.

³ iPATH.Berlin, Campus Benjamin Franklin, Charité - Universitätsmedizin Berlin, Corporate Member of Freie Universität Berlin, Humboldt-Universität zu Berlin, Berlin, Germany.

⁵ Department of Neurology, Brigham & Women's Hospital, Harvard Medical School, Boston, USA.

⁶ VIB Center for Brain and Disease Research at KU Leuven, Leuven, Belgium.

⁷ UK Dementia Research Institute@UCL, University College London, London, UK.

Short title: Presenilins in intestinal homeostasis

***Address correspondence to:**

Christoph Becker, PhD

Department of Medicine 1,

Friedrich-Alexander-University Erlangen-Nürnberg

Erlangen, Germany

Phone: (0049) 9131-85 35 886

Email: christoph.becker@uk-erlangen.de

32 **ABSTRACT**

33 **Objective:** Mutations in presenilin genes are the major cause of Alzheimer's disease.
34 However, little is known about their expression and function in the gut. In this study, we identify
35 the presenilins Psen1 and Psen2 as key molecules that maintain intestinal homeostasis.

36 **Design:** Human inflammatory bowel disease (IBD) and control samples were analyzed for
37 Psen1 expression. Newly generated intestinal epithelium-specific Psen1-deficient, Psen2
38 deficient and inducible Psen1/Psen2 double deficient mice were used to dissect the functional
39 role of presenilins in intestinal homeostasis.

40 **Results:** Psen1 expression was regulated in experimental gut inflammation and in IBD
41 patients. Induced deletion of Psen1 and Psen2 in mice caused rapid weight loss and
42 spontaneous development of intestinal inflammation. Mice exhibited epithelial barrier
43 disruption with bacterial translocation and deregulation of key pathways for nutrient uptake.
44 Wasting disease was independent of gut inflammation and dysbiosis, as depletion of
45 microbiota rescued Psen-deficient animals from spontaneous colitis development, but not from
46 weight loss. On a molecular level, intestinal epithelial cells lacking Psen showed impaired
47 Notch signaling and dysregulated epithelial differentiation.

48 **Conclusion:** Overall, our study provides evidence that Psen1 and Psen2 are important
49 guardians of intestinal homeostasis and future targets for barrier-promoting therapeutic
50 strategies in IBD.

51

52 **Keywords:** presenilins, intestinal epithelium, barrier breakdown, intestinal inflammation, IBD,
53 gamma-secretase, Notch, enterocytes, malnutrition

54 **WHAT IS ALREADY KNOWN ON THIS TOPIC**

- 55 ➤ An impaired epithelial barrier is observed in patients with IBD and disruption of the
56 intestinal epithelial monolayer induces gut inflammation in mice.
- 57 ➤ Many IBD patients experience weight loss and malnutrition.
- 58 ➤ Psen1 and Psen2 are key molecules in the pathogenesis of Alzheimer's Disease while
59 their role in the gut remains largely unknown.

60 **WHAT THIS STUDY ADDS**

- 61 ➤ This is the first study describing the functional role of Psen1 and Psen2 in intestinal
62 homeostasis.
- 63 ➤ Psen1 expression is impaired in the inflamed intestine of IBD patients and mice with
64 experimentally induced inflammation.
- 65 ➤ Inducible deletion of both presenilins in IECs results in spontaneous intestinal
66 inflammation with barrier breakdown and bacterial translocation.
- 67 ➤ Epithelial Psen1 and Psen2 are crucial molecules for Notch-mediated IEC
68 differentiation.
- 69 ➤ Mice with an IEC-specific deletion of Psen1/Psen2 develop lethal severe wasting.

70 **HOW THIS STUDY MIGHT AFFECT RESEARCH, PRACTICE OR**
71 **POLICY**

- 72 ➤ Since our study demonstrates that presenilin expression is pivotal for intestinal
73 homeostasis, we suggest the presenilins as promising future targets in IBD
74 pathogenesis for the improvement of barrier integrity and malnutrition.

75 INTRODUCTION

76 Presenilins are transmembrane proteins that act as the catalytic subunit of the gamma-
77 secretase complex, which plays a central role in the processing of amyloid precursor protein
78 (APP) and several other substrates, including the Notch receptor.[1–3] Apart from their central
79 role in the gamma-secretase complex, presenilins have also been implicated in autophagy,
80 apoptosis, protein trafficking, and calcium homeostasis, which appear to be independent of
81 gamma-secretase activity.[4] Presenilins are best known as critical players in the complex
82 pathogenesis of Alzheimer's disease (AD). Mutations in presenilin genes, particularly *PSEN1*
83 and *PSEN2*, are known to be responsible for a subset of early-onset familial AD cases.[5]
84 Although *PSEN1* and *PSEN2* share structural similarities and exhibit some functional overlap,
85 they also have distinct expression patterns and different substrate specificities.[6–8] Genetic
86 deletion of *Psen1* causes severe morphological defects in the developing brain and
87 hemorrhages, leading to the death of *Psen1*^{-/-} mice shortly after birth.[9] While studies on
88 *PSEN1* and *PSEN2* have largely focused on their role in neurologic diseases, far less is known
89 about the functional role of the presenilins in other organs, e.g. in the gut. Interestingly, recent
90 epidemiologic studies and experimental mouse models have uncovered a link between AD
91 and intestinal inflammation.[10–13] In this context, our own research data show dysregulation
92 of the presenilins in experimental colitis in mice, providing a rational for studying these
93 molecules in the gut.

94 For efficient protection of the gastrointestinal (GI) tract, intestinal epithelial cells (IECs) form a
95 highly effective barrier against potentially harmful microbes, toxins, and antigens, present in
96 the intestinal lumen. A tight control of IEC differentiation, proliferation, and cell death are key
97 to ensuring gut tissue homeostasis. Perturbations of epithelial homeostasis can lead to GI
98 pathologies, including the inflammatory bowel diseases (IBD) Crohn's disease (CD) and
99 ulcerative colitis (UC). Several pathways including Wnt- and Notch-signaling closely work
100 together to maintain tissue homeostasis and thus prevent IBD.[14] In addition to abdominal
101 pain and diarrhea, 70-80% of hospitalized IBD patients experience weight loss [15, 16] and
102 20-85% suffer from malnutrition.[17, 18] To date, the underlying mechanisms leading to IBD

103 and especially malnutrition are still incompletely understood. However, multiple factors have
104 been identified that contribute to disease pathology, including genetic and environmental
105 factors, such as alterations in the microbiome that induce the recruitment of mucosal immune
106 cells to the inflamed areas, ultimately leading to barrier defects.[19]

107 Given the pivotal role of presenilins in both mediating the processing of the Notch receptor [2,
108 20–22] and their interaction with the Wnt signaling pathway [23–26], we hypothesized that
109 presenilins might be crucially involved in intestinal homeostasis and inflammation.

110 In this study, we identified the presenilins Psen1 and Psen2 as important molecules in
111 maintaining intestinal homeostasis. While single deletions of *Psen1* or *Psen2* were fully
112 compensated by each other, the generation of inducible Psen1/2 double knockout mice
113 resulted in spontaneous development of intestinal inflammation with barrier breakdown and
114 subsequent bacterial translocation. Lack of Psen1 and Psen2 severely impaired IEC
115 differentiation with upregulation of secretory cells including goblet, Paneth, and
116 enteroendocrine cells, at the expense of absorptive enterocytes. Deletion of *Psen1* and *Psen2*
117 caused severe impairment of nutrient uptake ultimately leading to malnutrition and death of
118 these mice. While antibiotic treatment ameliorated gut inflammation, the weight loss of mice
119 was not reversed. Our study demonstrates that presenilin expression is pivotal for intestinal
120 homeostasis as it controls IEC differentiation and nutrient absorption, both of which contribute
121 to barrier maintenance.

122 **METHODS**

123 Methods are available as online supplemental file.

124 RESULTS

125 **Presenilins are expressed in the intestinal epithelium and are differentially** 126 **regulated during intestinal inflammation**

127 To identify underlying mechanisms of IBD pathogenesis, we sought to identify novel and
128 previously unrecognized pathways that might be involved in intestinal inflammation. To this
129 end, we initially performed bulk RNA sequencing comparing colonic tissue samples from mice
130 subjected to DSS-induced experimental colitis and healthy control animals. While several IBD-
131 related pathways, such as metabolism- and cytokine-related pathways were found by KEGG
132 pathway analysis, our colitis data surprisingly also revealed an enrichment of pathways
133 attributed to neurodegeneration such as those involved in Alzheimer's disease (**Fig. 1A**)
134 Among the differentially expressed genes in both pathways, we found the presenilins *Psen1*
135 and *Psen2*, which are key molecules in the genetics of familial AD (**Suppl. Fig. 1**).[27] Thus,
136 we next investigated *Psen1* expression levels during the course of DSS-induced colitis and
137 recovery.[28] Strikingly, *Psen1* gene expression was significantly downregulated during the
138 development of colitis, whereas expression levels returned to baseline levels during the
139 recovery phase (**Fig. 1B**). Downregulation of *Psen1* expression during intestinal inflammation
140 was also supported by assessing *Psen1* protein levels in inflamed colonic tissue from DSS-
141 treated mice (**Fig. 1C**). To compare the *Psen1* expression pattern between steady state
142 conditions and intestinal inflammation, immunofluorescence staining of *Psen1* was performed
143 in healthy and inflamed murine gut tissue. We found that *Psen1* expression at the steady-state
144 is mainly restricted to IECs, with low but detectable expression in the lamina propria. In
145 contrast, *Psen1* levels were reduced in the epithelium of DSS-treated mice during intestinal
146 inflammation (**Fig. 1D**). To elucidate whether the observed deregulation of *Psen1* can be
147 translated to human intestinal inflammation, *PSEN1* expression in gut samples of healthy
148 individuals was compared to those of UC and CD patients using a publicly available
149 transcriptomic dataset.[29] Consistent with the data from our mouse model, *PSEN1* expression
150 was significantly decreased in both IBD entities (**Fig. 1E**). Moreover, among our in-house

151 cohort of IBD patients, *PSEN1* was also significantly downregulated in the colon of both UC
152 and CD patients (**Fig. 1F**). Of note, *PSEN1* expression levels also correlated with disease
153 severity as shown in two different IBD cohorts (**Fig. 1G and H**). In contrast, the expression
154 levels of *PSEN2* mRNA remained unchanged in colonic samples of IBD patients examined in
155 our study (data not shown). To further confirm the observed downregulation of PSEN1 in
156 inflamed human tissues at the protein level, immunofluorescence staining for PSEN1 in human
157 IBD tissue samples was conducted. In line with the above data, this analysis showed a
158 downregulation of PSEN1 in UC and CD patients, when compared to healthy individuals (**Fig.**
159 **1I**). Taken together, our analysis demonstrates intestinal epithelial expression of Psen1,
160 together with marked deregulation during intestinal inflammation in mice and humans,
161 suggesting Psen1 as an important epithelial molecule involved in intestinal inflammation.

162 **Lack of epithelial Psen1 alone does not disrupt intestinal homeostasis**

163 To study potential functions of Psen1 in the mouse intestine, *Psen1^{fl/fl}* mice [30] were crossed
164 with villin-cre mice to generate mice with IEC-specific homozygous deletion of *Psen1*
165 (*Psen1^{ΔIEC}*) (**Suppl. Fig. 2A**). Successful IEC-specific deletion of Psen1 was proven at the
166 RNA and protein level in mouse gut tissue and in organoids generated from gut samples of
167 these mice (**Suppl. Fig. 2B – G**). Notably, homozygous *Psen1^{ΔIEC}* mice did not develop an
168 overt phenotype and no histological changes were observed in the intestinal architecture when
169 compared to their littermate controls (*Psen1^{fl/fl}* mice) (**Suppl. Fig. 3A**). In addition, mRNA and
170 protein analysis of IEC subtypes and differentiation markers revealed that IEC differentiation
171 from ISC into absorptive enterocytes or secretory cell types such as goblet, Paneth,
172 enteroendocrine or tuft cells, did not differ between the two groups (**Suppl. Fig. 3B-D**).
173 Moreover, no differences were observed in the levels of several inflammation-associated
174 factors (**Suppl. Fig. 3E**). This was further supported by bulk RNA sequencing of ileum and
175 colon tissue from *Psen1^{ΔIEC}* compared to control littermates, which confirmed that the lack of
176 Psen1 expression had no major impact on the gut transcriptome (**Suppl. Fig. 3F**). Interestingly,
177 however, Psen2 protein levels were significantly upregulated in the ileum and colon of

178 *Psen1*^{ΔIEC} mice (**Suppl. Fig. 3G**), suggesting a potential compensatory mechanism between
179 *Psen1* and *Psen2* in IECs.

180 **Inducible *Psen1/2* double knockout mice spontaneously develop intestinal** 181 **inflammation**

182 Since we hypothesized that intestinal epithelial *Psen2* can compensate for the loss of *Psen1*
183 in IECs, we crossed *Psen1*^{ΔIEC} with *Psen2*^{-/-} mice to generate *Psen1/2* double knockout mice
184 (**Suppl. Fig. 4A**). Noteworthy, general *Psen2*^{-/-} mice were utilized in this approach, because,
185 to the best of our knowledge, conditional *Psen2* knockout mice have not yet been established.

186 Remarkably, we did not obtain any *Psen1/2* double knockout mice, while the other expected
187 genotypes were born at increased ratios (**Suppl. Fig. 4B**). Of note, one allele of *Psen2* was
188 sufficient to maintain intestinal homeostasis, as *Psen1* knockout mice on a heterozygous
189 *Psen2* background (*Psen2*^{+/-} *Psen1*^{ΔIEC}) were born alive and showed no detectable changes in
190 gut architecture or intestinal epithelial differentiation (**Suppl. Fig. 4B – G**). Moreover, a detailed
191 analysis of the small and large bowel of *Psen2*^{-/-} mice [31] (**Suppl. Fig. 5A**) revealed no
192 detectable changes under steady-state conditions (**Suppl. Fig. 5B – G**). Together our data
193 demonstrated that neither the absence of *Psen1* nor that of *Psen2* alone affected gut tissue
194 homeostasis, while deletion of both presenilins caused early embryonic lethality.

195 To overcome the embryonic lethality of *Psen1/2* double knockout mice and to study the
196 functions of both genes in the gut, we established a new mouse line with an inducible *Psen1*
197 knockout allele on a background of a *Psen2* germline deletion (*Psen2*^{-/-} *Psen1*^{ΔIEC}; iDKO)
198 (**Suppl. Fig. 6A**). Successful deletion of *Psen1* on the *Psen2*^{-/-} background was achieved by
199 injection of tamoxifen (**Fig. 2A**) and greatly reduced expression levels of *Psen1* in IECs and
200 complete absence of *Psen2* in whole mouse ileal and colonic tissue samples as well as in
201 isolated organoids was confirmed at the mRNA and protein level (**Suppl. Fig. 6B – F**). In sharp
202 contrast to *Psen1* and *Psen2* single knockout mice, iDKO mice showed rapid and significant
203 weight loss starting on day five to six when compared to control *Psen2*^{-/-} *Psen1*^{fl/fl} littermate
204 mice, with termination criteria reached on day eight after the first tamoxifen injection (**Fig. 2B**).

205 In addition, endoscopy of the mice demonstrated the development of spontaneous colitis in
206 iDKO mice as assessed by the murine endoscopic index of colitis severity (MEICS) score (**Fig.**
207 **2C**).[32] Moreover, colon length measurements revealed a significant shortening of the colon
208 in iDKO mice compared to their littermate controls (**Fig. 2D**). Furthermore, histological
209 examination of the small and large intestine of the mice revealed pronounced histological
210 changes, including signs of inflammation and cell death (yellow arrows). In the ileum and
211 proximal colon, we observed structural changes in the epithelium accompanied by abundant
212 mucus production (black arrows) (**Fig. 2E**). In addition, Psen1/2 double deficient epithelial
213 organoids (**Suppl. Fig. 7A**) completely lacked the usual budded morphology and had a
214 significantly reduced size (**Suppl. Fig. 7B**), further supporting aberrant IEC-intrinsic
215 mechanisms in the absence of Psen1/2. Furthermore, assessment of the expression levels of
216 various pro-inflammatory factors, including *S100a9*, *Il1b*, and *Tnf*, revealed a striking
217 upregulation of these markers in the ileum and colon of iDKO mice compared to littermate
218 controls (**Fig. 2F**). Moreover, assessment of immune cell infiltration revealed significantly
219 increased numbers of neutrophils as determined by myeloperoxidase (MPO) staining in the
220 ileum and colon of iDKO mice, as well as significantly increased numbers of macrophages as
221 determined by F4/80 staining in the ileum of iDKO mice (**Fig. 2G**). In conclusion, our data
222 demonstrate that the presenilins are key factors for intestinal homeostasis, as dual deletion of
223 Psen1 and Psen2 leads to the development of spontaneous intestinal inflammation *in vivo*.

224 **Presenilins are key to intestinal barrier function**

225 Intestinal barrier breakdown is considered as the key factor underlying the
226 immunopathogenesis of IBD.[33] To investigate whether Psen deficiency affects intestinal
227 barrier functions, iDKO and control (*Psen2*^{-/-} *Psen1*^{fl/fl}) littermate animals were orally gavaged
228 with FITC-Dextran to determine its passage across the epithelium. Interestingly, significantly
229 higher levels of FITC-Dextran were measured in the serum of iDKO mice compared to their
230 littermate controls, suggestive of substantial barrier defects (**Fig. 3A**). To investigate whether
231 Psen deficiency-induced epithelial barrier disruption is independent of the cellular or microbial
232 microenvironment, intestinal epithelial organoids were incubated with lucifer yellow to track its

233 passage into the organoid lumen.[34] An increase in dye intensity in the lumen of organoids
234 generated from iDKO but not control mice was observed, indicating that the observed barrier
235 breakdown due to presenilin loss is IEC intrinsic and independent of the intestinal environment
236 (**Fig. 3B**). Adherens junction and tight junction proteins, such as E-Cadherin and occludin
237 respectively, regulate paracellular permeability and are key guardians of the epithelial
238 barrier.[35] Several studies have already shown a downregulation of these components in both
239 UC and CD patients.[36, 37] Interestingly, immunofluorescence staining in ileal and colonic
240 tissue samples from tamoxifen-injected control and iDKO mice showed a strong reduction of
241 E-Cadherin in the membranous portion of IECs in iDKO mice (**Fig. 3C**). Moreover, Western
242 blot analysis revealed a loss of full-length occludin in the ileum of the mice, along with reduced
243 levels of cleaved occludin in the ileum and colon of iDKO mice (**Fig. 3D**). When sacrificing
244 iDKO mice at different timepoints after the first dose of tamoxifen, we determined that full-
245 length occludin was completely abolished already on day five, while the cleaved form of
246 occludin was reduced on day seven after the first tamoxifen injection (**Fig. 3E**). These
247 observations were supported by small intestinal organoid cultures (**Suppl. Fig. 7C**), suggesting
248 that epithelial-intrinsic mechanisms lead to reduced occludin expression upon presenilin
249 deletion. To functionally analyze the consequences of intestinal barrier dysfunction on
250 microbial dysbiosis in Psen iDKO mice, gut tissue sections were stained with a fluorescent
251 FISH probe detecting all eubacteria. Strikingly, while bacteria in control animals were well
252 separated from the epithelial lining, bacteria in iDKO mice infiltrated the crypt area down to the
253 crypt bottom and even into the normally tight IEC monolayer (**Fig. 3F**), suggesting that
254 presenilins are key to maintain an efficient barrier and to prevent microbial colonization of the
255 crypt regions. To examine the systemic impact of the previously observed intestinal barrier
256 breakdown in iDKO mice, tissue lysates of mesenteric lymph nodes (MLN) and livers from the
257 animals were plated on agar plates under aerobic and anaerobic conditions. While no colony-
258 forming units (CFUs) were detected in the tissues of control mice, high numbers of CFUs were
259 observed in the MLN and liver of iDKO mice (**Fig. 3G**), indicating that a Psen deficient gut
260 epithelium loses its ability to prevent a systemic spread of bacteria. In support of this,

261 examination of serum TNF- α levels indicated a systemic inflammatory response in iDKO mice,
262 as evidenced by significantly elevated TNF- α levels in mice deficient in both presenilins (Fig.
263 3H). To further validate these findings, levels of pro-inflammatory markers were assessed in
264 spleen tissue, revealing a marked increase of *Tnf* and *Nos2* (Fig. 3I). Finally, measurements
265 of serum aspartate aminotransferase (AST) and alanine aminotransferase (ALT) levels
266 indicated liver damage (Fig. 3J). In conclusion, our analysis clearly demonstrated a key role
267 of presenilins in barrier integrity, where deletion of both presenilins leads to alteration of E-
268 Cadherin distribution, loss of the tight junction protein occludin, subsequent breakdown of the
269 intestinal barrier and bacterial translocation to distant organs, eliciting a systemic inflammatory
270 response.

271 **Spontaneous inflammation but not rapid body weight loss in presenilin-deficient** 272 **mice is driven by microbiota**

273 To investigate whether barrier breakdown with subsequent bacterial translocation could be
274 chiefly responsible for severe wasting disease and early death of mice lacking *Psen1* and
275 *Psen2* in the epithelium, mice were pre-treated with an established antibiotic cocktail to deplete
276 the microbiota (Fig. 4A), which was confirmed by plating stool lysates before and after
277 antibiotic treatment and assessing the number of CFUs (Fig. 4B). Unexpectedly, daily weight
278 measurements revealed that iDKO mice treated with antibiotics displayed similar wasting
279 disease as iDKO mice subjected to normal water (Fig. 4C). In contrast, endoscopic scoring of
280 colitis severity revealed a significant reduction of inflammation in antibiotic-treated iDKO mice
281 compared to iDKO mice receiving water only (Fig. 4D). Furthermore, histological examination
282 of ileal and colonic tissue sections further confirmed the amelioration of inflammation in the
283 colon (Fig. 4E and F). In addition, antibiotic treatment significantly reduced the levels of pro-
284 inflammatory factors, including *Il6*, *Tnf*, *Il1b*, and *S100a9* in the ileum and colon of iDKO
285 compared to water-drinking iDKO mice (Fig. 4G). Taken together, antibiotic treatment of iDKO
286 mice could ameliorate signs of inflammation and barrier breakdown, but could not rescue the
287 weight loss in these mice, suggesting that microbial translocation in iDKO is a driver of colitis

288 development, but there might be another potential mechanism that underlies the rapid and
289 severe unrecoverable weight loss.

290 **Psen1 and Psen2 deficiency disrupts Notch signaling, alters IEC differentiation**
291 **and leads to malnutrition in inducible Psen1/2 double knockout mice**

292 To further improve our mechanistic understanding of the functions of presenilins in gut
293 homeostasis, we performed bulk RNA sequencing with ileal tissue lysates of iDKO mice and
294 control (*Psen2*^{-/-} *Psen1*^{fl/fl}) littermates. Interestingly, this analysis revealed broad Psen-
295 dependent transcriptional changes with 4129 differentially expressed genes between the two
296 groups (**Fig. 5A**). Using gene ontology analysis, we observed an upregulation of pathways
297 involved in inflammatory responses, cell migration and mucin type O-glycan biosynthesis in
298 iDKO mice. In contrast, numerous pathways related to transport and absorption of various
299 nutrient components, including lipids, ions, fat, sodium and minerals, were significantly
300 reduced in the ileum of iDKO mice (**Fig. 5B, Suppl. Tab. 1 and 2**). Moreover, metabolic
301 signatures, including lipid and fatty acid metabolic pathways, TCA cycle, gluconeogenesis, and
302 glycolysis, were also reduced in the intestine upon induced presenilin deletion. Ingenuity®
303 Pathway Analysis further revealed increased signatures of cell migration, epithelial cell
304 differentiation and tumorigenic pathways, as well as decreased uptake, transport, oxidation,
305 synthesis and metabolism of lipids and fatty acids (**Suppl. Fig. 8A and Suppl. Tab. 3**). By
306 analyzing epithelial cell differentiation in more detail, we observed an influence of dual
307 presenilin deletion on secretory IEC differentiation, with increased numbers of goblet, Paneth,
308 and enteroendocrine cells (**Suppl. Fig. 8B**). To thoroughly analyze the different IEC types,
309 several immunofluorescence stainings for unique IEC type marker proteins were performed.
310 Remarkably, immunofluorescence staining for different stem cell markers showed a significant
311 loss of Olfm4⁺ and Lgr5⁺ stem cell populations in the ileum and colon of iDKO mice.
312 Furthermore, using Ki67, we detected significantly reduced numbers of proliferating cells in
313 ileal and colonic tissue sections from iDKO mice compared to control littermates (**Suppl. Fig.**
314 **8C**). In addition, this analysis further confirmed a significant upregulation of the number of

315 secretory cells, including Paneth, goblet, and enteroendocrine cells (**Suppl. Fig. 8D**). Similar
316 results were obtained *in vitro* using small intestinal organoid cultures generated from these
317 mice, showing impaired IEC differentiation with increased numbers of secretory cells and
318 decreased numbers of stem cells along with reduced proliferation (**Suppl. Fig. 7D and E**). In
319 contrast, our RNA sequencing approach revealed a striking downregulation of genes
320 associated with absorptive enterocytes (**Fig. 5C**). In line with this, staining for the enterocyte-
321 specific marker intestinal alkaline phosphatase (IAP) revealed a largely diminished number of
322 absorptive enterocytes in the small intestine of iDKO mice (**Fig. 5D**). To functionally investigate
323 the loss of enterocytes in the intestine of inducible Psen1/2 double knockout mice, serum
324 glucose measurements revealed a highly significant downregulation of glucose levels in iDKO
325 mice (**Fig. 5E**), suggesting that the lack of Psen1/2 diminishes the ability of the intestine to
326 properly absorb vitally important nutrients. To test whether the impaired uptake rate is IEC-
327 specific, small intestinal organoids from control and iDKO mice were treated with Rhodamine
328 123, a commonly used tracer dye to investigate transport rates. Interestingly, while small
329 intestinal organoids from control mice were able to take up Rhodamine 123 into the lumen,
330 small intestinal organoids generated from iDKO mice almost completely failed to take up
331 Rhodamine 123 (**Fig. 5F**). As further evidence of impaired intestinal glucose absorption *in vivo*,
332 an oral glucose tolerance test was performed in control and iDKO mice. Remarkably, this test
333 revealed severely impaired intestinal glucose uptake rates in iDKO mice compared to control
334 mice (**Fig. 5G**). Notably, antibiotic-treated iDKO mice still exhibited significantly reduced serum
335 glucose levels (Suppl. 9A) and impaired intestinal glucose uptake rates in an oral glucose
336 tolerance test (Suppl. Fig. 9B), suggesting that the observed changes in systemic energy
337 metabolism are not directly related to intestinal inflammation. Based on the observation by
338 Tang *et al.* that the average adipocyte area in mesenteric white adipose tissue is almost
339 completely reduced in fasted mice [38], we analyzed the mesenteric white adipose tissue of
340 iDKO mice and compared it with littermate controls. The average adipose area was drastically
341 reduced in inducible Psen1/2 double knockout mice (**Fig. 5H**). We reasoned that this was likely
342 due to reduced lipid uptake given that the number of absorptive enterocytes was reduced. To

343 test this hypothesis in a functional approach *in vivo*, fasted mice received corn oil as a lipid
344 source by oral gavage. Application of corn oil has been shown to result in lipid droplet formation
345 due to uptake of lipids by absorptive enterocytes, which can be detected by
346 immunofluorescence staining.[39] Strikingly, the lipid droplet accumulation in the IECs of the
347 small intestine was completely blocked in iDKO mice compared to littermate controls (**Fig. 5I**).
348 Finally, to evaluate the state of liver energy stores, we employed Periodic Acid-Schiff (PAS)
349 staining to detect glycogen levels in liver tissue of the mice. Remarkably, our analysis unveiled
350 a substantial decrease in glycogen content within the liver of iDKO mice when compared to
351 control mice (Fig. 5J). These analyses ultimately highlight the severity of the presenilin-
352 dependent loss of absorptive enterocytes, suggesting that the death of the inducible Psen1/2
353 double knockout mice may be due to malnutrition.

354 Since the γ -secretase multi-protein complex is critically involved in Notch signaling [20, 22, 40],
355 we hypothesized that non-functional Notch signaling might be responsible for the severely
356 impaired IEC differentiation in the inducible Psen1/2 double knockout mice, leading to reduced
357 barrier permeability on the one hand and malnutrition on the other hand. To test whether Notch
358 signaling is impaired in the intestine upon double presenilin deficiency, we performed Western
359 blot analysis using the Notch intracellular domain (NICD) as a marker of functional Notch
360 signaling. Remarkably, whereas Notch was still cleaved and NICD was released in Psen1 and
361 Psen2 single knockout mice, NICD levels were completely abolished in the colon, ileum, and
362 in small intestinal organoids generated from iDKO mice (**Fig. 5K and Suppl. Fig. 7F**). This
363 could explain the observed lack of phenotype in heterozygous Psen1/2 double knockout mice,
364 showing that one allele of Psen2 is sufficient to maintain functional Notch signaling (**Suppl.**
365 **Fig. 4H**).

366 Overall, our study identified the presenilins Psen1 and Psen2 as previously unknown players
367 in intestinal homeostasis and inflammation, where they act as key molecules in maintaining
368 balanced IEC differentiation and barrier function integrity to prevent malnutrition and intestinal
369 inflammation (**Suppl. Fig. 9C and Fig. 5L**). Thus, supporting presenilin enzymatic activity in
370 the gut epithelium or downstream signaling may provide new targets for novel IBD therapies.

371 DISCUSSION

372 Our study reveals for the first time the key role of the presenilins Psen1 and Psen2 for intestinal
373 homeostasis by controlling the balance of IEC differentiation to sustain barrier integrity and to
374 avoid malnutrition and the development of intestinal inflammation. To date, presenilins have
375 been extensively studied in the brain, where several loss-of-function mutations in presenilin
376 genes can cause Alzheimer's disease. Although many different studies have investigated the
377 role of Notch signaling and general γ -secretase activity in intestinal homeostasis and
378 inflammation, not much is known about how the presenilins are regulated during intestinal
379 health and disease and whether they are critically involved in these processes. Interestingly,
380 our group has already established a link between *Psen1* expression in intestinal epithelial cells
381 and colorectal tumor development.[41] Remarkably, our present study identifies both
382 presenilins as key molecules in intestinal homeostasis and inflammation. Strikingly, double
383 deletion of Psen1 and Psen2 in mice leads to spontaneous development of intestinal
384 inflammation, with barrier breakdown and bacterial translocation. These outcomes are
385 associated with impaired IEC differentiation, non-functional Notch signaling, ultimately
386 resulting in malnutrition and death of the inducible Psen1/2 double knockout mice.

387 To date, the role of Notch signaling in intestinal inflammation is controversial. While some
388 animal studies have shown pro-inflammatory effects of Notch signaling, as for example by
389 using different γ -secretase inhibitors that reduced colitis severity in DSS- or TNBS-treated mice
390 [42, 43], other studies have demonstrated anti-inflammatory roles of Notch signaling during
391 colitis. For example, IEC-specific deletion of *Rbpj*, the major transcriptional effector of Notch
392 signaling, in mice resulted in spontaneous development of chronic colitis with accumulation of
393 Th17 cells [44], and deletion of Notch-1 led to more severe colitis development in DSS-treated
394 mice.[45] Surprisingly, various studies reported a significant increase in Notch signaling in IBD
395 patients.[46–49] However, rather than being harmful by contributing to the severity of the
396 disease, these changes may be beneficial by helping to regenerate the damaged epithelium
397 and thus recover from the disease.[46] Notably, several clinical trials using different γ -
398 secretase specific inhibitors for the treatment of various diseases, including cancer and

399 Alzheimer's disease, have described the development of spontaneous gut inflammation, even
400 grade 3 colitis with ulceration in some of the patients.[50–54] These findings in humans support
401 our observation in *Psen1/2* double knockout mice and our data therefore provide a potential
402 mechanistic explanation for the observed side effects in these patients. In this context, our
403 current study demonstrates the severity of double presenilin deletion in the intestine, leading
404 to the death of the mice within a few days, thus highlighting the need to avoid double presenilin
405 inhibition by γ -secretase inhibitors in the treatment of Alzheimer's disease or tumors.
406 Moreover, our study demonstrates the existence of compensatory mechanisms between the
407 two presenilins in the gut, which could be exploited to avoid Notch-related off-target effects,
408 especially in the intestine. This knowledge could be used in the future when designing new γ -
409 secretase inhibitors. Interestingly, Sannerud *et al.* described that PSEN2 exhibits an additional
410 structural motif in mouse embryonic fibroblasts, which is absent PSEN1. As a result, PSEN2-
411 containing γ -secretases are directed towards late endosomes/lysosomes, while PSEN1-
412 containing γ -secretases, are primarily located at the plasma membrane, thus contributing to a
413 broader subcellular localization.[6, 7] Therefore, future studies should aim to study the
414 subcellular localization of PSEN1 and PSEN2 in the IECs to better understand how
415 compartmentalization of PSEN1 and PSEN2 affects their functions in the gut epithelium.
416 Functional tight junctions are normally formed between goblet cells and enterocytes, strictly
417 limiting permeability.[55] Interestingly, the depth of tight junction formation and the number of
418 tight junction strands depend on the different IEC types between which they are formed.[56]
419 This suggests that functionally different tight junctions may be formed in the inducible *Psen1/2*
420 double knockout mice.
421 Interestingly, although many publications have addressed the role of Notch signaling in
422 intestinal homeostasis by IEC-specific deletion of various Notch signaling components, quite
423 different phenotypes have been observed. For example, while single *Notch1* or *Notch2*
424 knockout mice and single *Dll1* and *Dll4* knockout mice show no phenotype, dual deletion of
425 *Notch1/Notch2* or *Dll1/Dll4* resulted in increased goblet cell numbers and decreased
426 proliferative cells.[57, 58] Similarly, compensatory mechanisms were observed among *Hes*

427 genes, whereas triple deletion of *Hes1/Hes3/Hes5* resulted in increased secretory cell
428 numbers and decreased proliferation.[59] Moreover, deletion of the α -secretase Adam10 also
429 resulted in the phenotypes described above.[60] Remarkably, IEC-specific deletion of *Rbpj* not
430 only upregulates secretory cell lineage and downregulates proliferation but also induces
431 spontaneous colitis and bacterial translocation.[44] Notably, none of these studies investigated
432 the loss of absorptive enterocytes and associated malnutrition as seen in the mouse model
433 presented in the current study. On the one hand, these studies demonstrate the importance of
434 compensatory mechanisms within protein families to ensure the proper functioning of vitally
435 important pathways. More importantly, they suggest γ -secretase independent functions
436 beyond their involvement in Notch signaling, which has been also previously observed for the
437 presenilins [4], further highlighting the crucial importance of the presenilins in maintaining
438 intestinal homeostasis, particularly nutrient uptake and barrier function. At present, it is well-
439 established that IBD pathogenesis and malnutrition are closely linked and are thought to result
440 from reduced oral food intake, enteric nutrient loss, increased energy requirements, and
441 malabsorption.[61] Importantly, malnutrition has even been described to be associated with
442 poor clinical outcome in IBD patients.[62, 63] Malabsorption in these patients is thought to be
443 due to loss of epithelial integrity and impaired epithelial transport [61], but the underlying
444 molecular mechanisms are poorly understood. Thus, our study suggests a molecular origin for
445 the commonly observed reduced nutrient absorption and thus malnutrition in IBD patients,
446 involving the loss of the intestinal epithelial presenilins. To date, GWAS studies have not
447 identified presenilins or other important Notch signaling-related molecules as being associated
448 with IBD pathogenesis.[64, 65] This might be due to the high degree of redundancy often
449 reported for these molecules. In contrast to Psen1, our data from experimental colitis and IBD
450 patients did not reveal a downregulation of Psen2. Additionally, not all publicly available
451 transcriptomic datasets showed a downregulation of presenilin expression, suggesting that the
452 expression of presenilins may vary depending on the disease, stage, sampling, and
453 therapeutic intervention. Given that presenilin expression can be influenced by various IBD-
454 related cytokines, including TNF- α (data not shown), it is crucial to consider the impact of

455 biologics used as treatment options in these patients. Moreover, presenilin function is not only
456 regulated on a transcriptional level but can also be activated by post-translational modification,
457 such as phosphorylation. For example, Protein Kinase A, which has been reported to mediate
458 presenilin phosphorylation [66], is significantly downregulated in UC patients (data not shown).
459 Future studies will be necessary to establish pharmacological approaches that could target
460 presenilin as a treatment option for IBD. These could involve targeting the epithelium in
461 agonistic approaches promoting presenilin enzymatic activity.

462 In conclusion, our research identifies the presenilins as key molecules of intestinal
463 homeostasis by coordinating a balanced IEC differentiation and thus a tight intestinal barrier.
464 In contrast, impaired expression or function of presenilins can lead to Notch signaling
465 disruption, with impaired IEC differentiation, resulting in malnutrition, barrier breakdown and
466 ultimately the development of spontaneous inflammation. In the future, these findings may be
467 useful in the development of IBD treatment strategies.

468 MATERIAL AND METHODS

469 Human material

470 Human specimens were obtained from the Department of Gastroenterology, Infectious
471 Diseases and Rheumatology of the Charité - Universitätsmedizin Berlin, and the
472 Universitätsklinikum Erlangen, after written informed consent of the patients and approval by
473 the Ethics Committee of the Charité - Universitätsmedizin Berlin and the Ethics Committee of
474 the Universitätsklinikum Erlangen. Colon specimens from healthy and IBD patients were
475 embedded in paraffin and subsequently stained as described below. Data were anonymized.
476 Patient's clinical information is shown in **Suppl. Tab. 4**.

477 Mice

478 Mice carrying loxP-flanked *Psen1* alleles (*Psen1^{fl/fl}*) (Jackson strain #004825) were crossed
479 with villin-cre mice (Jackson strain #004586) to generate mice with a homozygous conditional
480 deletion of *Psen1* in IECs (*Psen1^{ΔIEC}*). The generation and maintenance of *Psen2^{-/-}* has been
481 described previously (Jackson strain #005617). *Psen1^{fl/fl}* and *Psen2^{+/+}* mice were used as
482 littermate controls, respectively. *Psen1^{ΔIEC}* were further crossed with *Psen2^{-/-}* to generate
483 *Psen2^{+/-} Psen1^{ΔIEC}* mice. In addition, *Psen1^{fl/fl}* mice were crossed with *Psen2^{-/-}* and villin-
484 creERT2 (Jackson strain #020282) to generate inducible *Psen1/2* double knockout mice
485 (*Psen2^{-/-} Psen1^{ΔIEC}*; iDKO). iDKO mice were compared to *Psen2^{-/-} Psen1^{fl/fl}* mice as littermate
486 controls in all experiments. All mice were routinely screened for pathogens according to
487 FELASA guidelines. Animals were sex- and age-matched and littermates were used for each
488 experiment in accordance with German law and with the approval of the local animal care
489 committee. Sample size was calculated using G*Power.[67]

490 Histology scoring

491 Pathological scoring was performed on hematoxylin & eosin-stained tissue sections. The
492 scoring included evaluating the integrity of the intestinal epithelium (0: intact; 1-3: mild,
493 moderate or severe destruction, respectively) and mucosal inflammation (0: no inflammatory
494 infiltration; 1-3: rare, moderate or massive inflammatory infiltration, respectively).

495 **Endoscopic evaluation**

496 Endoscopic evaluation was performed using high-resolution mouse video endoscopy as
497 previously described.[32] The murine endoscopic index of colitis severity score (MEICS)
498 evaluates colonic wall thickening, changes in normal vascular pattern, presence of fibrin,
499 mucosal granularity, and stool consistency. Scores ranged from 0 to 3 for each parameter, and
500 the sum of all the parameters is displayed as MEICS. The colon was scored for visible damage
501 by a blinded observer.

502 **Tamoxifen administration**

503 Inducible Psen1/2 double knockout mice were injected intraperitoneally (i.p.) with 75 mg/kg
504 tamoxifen (Sigma) diluted 1:1 in sunflower oil on 5 consecutive days.

505 **FITC-Dextran administration**

506 FITC-dextran administration was performed after the mice were fasted for 4 hours. 0.4 mg/kg
507 body weight of FITC-dextran (4,000 g/mol average molecular weight; Sigma) was administered
508 by oral gavage. After 4 hours, the mice were sacrificed, and serum FITC-dextran levels were
509 measured using a fluorimeter.

510 **Antibiotic treatment**

511 For microbiome depletion, mice were treated with 1 g/l metronidazole (Braun), 1 g/l ampicillin
512 (ratiopharm), 0.5 g/l vancomycin (Dr. Friedrich Eberth Arzneimittel GmbH), and 1 g/l neomycin
513 (Caelo) in drinking water. 8 g/l sweetener (Splenda®) was added to mask the bitter taste of the
514 antibiotics.

515 ***In vivo* HCS LipidTOX assay**

516 Mice were fasted for 4 hours and then given 200 µl of corn oil (Sigma) by oral gavage. After 4
517 hours, the mice were sacrificed. Cryosections were fixed in 4% PFA for 30 min and lipid
518 droplets were detected with HCS LipidTOX Green (1:200; Thermo Fisher). Nuclear staining
519 was performed with Hoechst (1:500; Invitrogen) and slides were mounted with fluorescence
520 mounting medium (Dako).

521 **Bacterial translocation studies**

522 Bacterial translocation was assessed by plating mesenteric lymph node (MLN) and liver tissue
523 lysates diluted in sterile PBS on MacConkey (Roth) and blood agar (Merck) plates to determine
524 colony forming units (CFU) under aerobic and anaerobic conditions after 24 hours of incubation
525 at 37°C. CFU were normalized to the organ weight. The anaerobic condition was established
526 using Anaerocult™ A (Merck).

527 **Serum glucose measurement**

528 Serum glucose was measured using a blood glucose meter (Ascensia Diabetes Care
529 Deutschland GmbH).

530 **Oral glucose tolerance test**

531 For the oral glucose tolerance test, mice were fasted overnight and baseline glucose levels
532 were measured using a blood glucose meter (Ascensia Diabetes Care Deutschland GmbH).
533 Mice then received 2.5 g glucose/kg body weight by oral gavage and blood glucose levels were
534 measured 10, 15, 20, 30, 45, 60, and 90 minutes later using a blood glucose meter.

535 **Murine organoid culture**

536 Small intestinal organoids were established as previously described.[68] Briefly, mice were
537 sacrificed, and the intestine was cut into small pieces, incubated in 2 mM EDTA for 30 minutes,
538 and the released epithelial cells were filtered through a 70 µm filter. Epithelial cells were then
539 plated in Cultrex (Bio-Techne) and cultured in culture medium in 5% CO₂ at 37°C and passaged
540 twice a week. Psen1 was deleted in small intestinal organoids by incubation with 50 ng/ml
541 tamoxifen for 5 days, organoids were split on day 3 and fresh tamoxifen was added.

542 **Organoid permeability assay**

543 Organoids were incubated with 1 mM Lucifer yellow (Sigma) for 1 hour at 37°C. 2 mM EGTA
544 incubated for 10-15 minutes at 37°C was used as a positive control. Images were captured
545 using a confocal microscope and images were analyzed using ImageJ as previously
546 described.[34]

547 **Rhodamine 123 uptake assay**

548 Organoids were incubated with 100 μ M Rhodamine 123 (Sigma) for 5 minutes at 37°C, washed
549 and incubated in basal organoid culture medium for another 40 minutes at 37°C. Images were
550 captured by confocal microscopy and analyzed using ImageJ.

551 **Histology and immunofluorescence staining**

552 For evaluation of histomorphology, tissue was formalin-fixed and embedded in paraffin.
553 Sections were cut from paraffin blocks and histochemically stained with hematoxylin and eosin.
554 Immunofluorescence staining was performed on formalin-fixed paraffin-embedded sections or
555 cryosections. Cryosections and organoid cultures were fixed with 4% PFA for 30 minutes at
556 room temperature and then washed with TBS-T for 5 minutes. For paraffin sections, sections
557 were incubated for 1 hour at 65°C, paraffin was removed with ROTI®Histol, and sections were
558 rehydrated in a decreasing ethanol row. Antigen retrieval was performed using Tris/ETDA at
559 450 W for 20 minutes. After cooling, the slides were incubated with 0.1% Triton X-100 for 10
560 minutes, washed in TBS-T, and the endogenous biotin-binding sites were blocked using the
561 Avidin/Biotin Blocking Kit (Vector Laboratories). The following primary antibodies were
562 incubated overnight at 4°C: Psen1 (1:300; #5643; Cell Signaling), E-Cadherin:FITC (1:200;
563 #612130; BD Biosciences), Olfm4 (1:300; #39141; Cell Signaling), Lysozyme (1:300; A0099 ;
564 Dako), Muc2 (1:500; NBP1-31231; Novus), Chromogranin A (1:300; NB120-15160; Novus),
565 Dcamk11 (1:200; ab31704; abcam), Ki67 (1:200; 14-5698-82; eBioscience), MPO (1:200;
566 #ab9535; abcam), F4/80 (1:200; #70076; Cell Signaling), Cl. Caspase 3 (1:300; #9662; Cell
567 Signaling), E-Cadherin (1:300; #3195; Cell Signaling), Occludin (1:300; #91131; Cell
568 Signaling), and ULEX (1:50; FL-1061-2; Vector Laboratories). The next day, the slides were
569 washed three times in TBS-T and incubated with the appropriate secondary antibodies (Alexa
570 Fluor®555 anti-rabbit: 1:200, BioLegend, # 406412 for Olfm4, Lysozyme, Muc2, ChgA,
571 Dcamk11 and Ki67; Biotin anti-rabbit IgG: 1:400, Jackson ImmunoResearch, # 111-065-144
572 combined with Streptavidin DyLight500: 1:400, Thermo Fisher, # 84542 for Psen1, MPO,
573 F4/80, Cl. Casp. 3, E-Cadherin and occludin) for 2 hours at room temperature. Slides were
574 washed in PBS, nuclear staining was performed with Hoechst (1:500; Invitrogen), and slides
575 were mounted with fluorescence mounting medium (Dako).

576 **Immunohistochemistry**

577 For immunohistochemical staining, small intestinal organoids were pelleted, embedded in
578 Histogel (Thermo Fisher), and then embedded in paraffin. Paraffin sections were incubated for
579 1 hour at 65°C, paraffin was removed with ROTI®Histol, and sections were and rehydrated in
580 a decreasing ethanol row. Antigen retrieval was performed using Tris/EDTA at 450 W for 20
581 minutes in a microwave. Endogenous peroxidase blocking was performed using 3% hydrogen
582 peroxide. Endogenous biotin-binding sites were blocked using the Avidin/Biotin Blocking Kit
583 (Vector Laboratories). The primary Psen1 antibody (1:300; #5643; Cell Signaling) was
584 incubated overnight at 4°C. The next day, slides were washed in PBS and the secondary
585 antibody (SignalStain®Boost IHC detection reagent (HRP, rabbit)) was incubated for 30
586 minutes at room temperature, followed by signal detection (SignalStain®DAB Chromogene
587 Substrate; SignalStain®DAB Diluent) for 8 minutes at room temperature. Counterstaining was
588 performed with hematoxylin for 5 seconds and washed with tap water. Sections were
589 dehydrated through an increasing ethanol series and mounted with Entellan (Merck).

590 **Intestinal alkaline phosphatase staining**

591 Alkaline phosphatase staining was performed on cryosections fixed in ice-cold acetone for 5
592 minutes. Sections were air dried for 5 minutes and incubated for 30 minutes at 37°C alkaline
593 phosphatase working solution: 0.2 M TRIS, 0.1M HCl, 0.01 g Naphtol AS-MX Phosphate
594 (Sigma) in 500 µl N,N Dimethylformamide (Merck), 0.036 g Fast Red Violet LB Salt (Sigma),
595 total pH = 8.74.

596 **Periodic Acid-Schiff staining**

597 PAS staining was performed on formalin-fixed, paraffin-embedded tissue sections. Paraffin
598 sections were incubated for 1 hour at 65°C, paraffin was removed with ROTI®Histol, and
599 sections were rehydrated in a decreasing ethanol series. Samples were then oxidized in 0.5%
600 periodic acid (Carl Roth) for 5 minutes, rinsed in distilled water, and incubated in Schiff's
601 reagent for 15 minutes (Carl Roth). After washing in tap water, the slides were counterstained
602 with hematoxylin for 1 minute. After further washing in tap water, the sections were dehydrated
603 and mounted with Entellan (Merck).

604 **In situ Hybridization**

605 For bacterial detection, the Eub338 probe was stained on formalin-fixed, paraffin-embedded
606 tissue sections. Paraffin sections were incubated for 1 hour at 65°C, paraffin was removed with
607 ROTI®Histol, and sections were rehydrated in a decreasing ethanol series. Slides were then
608 incubated in hybridization buffer for 20 minutes at room temperature, followed by incubation
609 with the Eub338 probe (3'-GCT GCC TCC CGT AGG AGT-5' Cy3; biomers) diluted 1:10 in
610 hybridization buffer for 90 minutes at 46°C in a hybridization oven as previously described.[69]
611 Counterstaining was performed with Hoechst (1:500; Invitrogen), and slides were mounted
612 with fluorescence mounting medium (Dako).

613 **RNAScope**

614 RNAScope® (ACDBio) staining was performed on formalin-fixed paraffin-embedded sections
615 according to the manufacturer's instructions. Briefly, sections were incubated for 1 hour at
616 65°C, paraffin was removed with ROTI®Histol, and sections were incubated in 100% ethanol.
617 Tissues were air dried, pretreated with hydrogen peroxide (ACDBio), and then heated at 100°C
618 for 15 minutes in Target Retrieval Buffer (ACDBio). This was followed by incubation at 40°C
619 for 30 minutes in a HybEZ™ Oven (ACDBio) with Protease Plus Reagent (ACDBio), after
620 which the slides were washed and a murine Lgr5 probe (ACDBio) was applied and incubated
621 at 40°C for 2 hours. Signal amplification and detection were performed using RNAScope® 2.5
622 HD Red Detection Reagent (ACDBio) according to the manufacturer's instructions. Nuclei were
623 detected with Hoechst (1:500; Invitrogen) and slides were mounted with fluorescence
624 mounting medium (Dako).

625 **Microscopy**

626 Images of staining were obtained using a NanoZoomer 2.0 (Hamamatsu), a DMI 4000 B
627 (Leica), or a DMI 6000 CS (Leica) microscope.

628 **Western blotting**

629 Tissue and organoid protein extracts were isolated using Tissue or Mammalian Protein
630 Extraction Reagent (Thermo Fisher). Protein concentration was determined by the Bradford

631 assay. Protein samples were diluted in NuPage LDS Sample Buffer (Thermo Fisher),
632 denatured at 95°C for 5 minutes, and then separated on Mini-PROTEAN® Precast Gels (Bio-
633 Rad) at 200 V for approximately 30 min. Proteins were blotted onto PVDF membranes, blocked
634 in 5% milk and incubated with the following antibodies at 4°C overnight: Psen1 (#5643; Cell
635 Signaling), Psen2 (#9979; Cell Signaling), Na-K-ATPase (#3010; Cell Signaling), Lamin A/C
636 (615802; Biolegend), GAPDH (#2118; Cell Signaling), β -actin HRP (ab49900; abcam),
637 Lysozyme (A0099; Dako), Occludin (#91131; Cell Signaling), NICD (#4147; Cell Signaling).
638 The next day, the membrane was incubated with the appropriate HRP-conjugated secondary
639 antibody (Cell Signaling) and developed on an Amersham™ Imager 800 (GE Healthcare Life
640 Sciences) using Western Lightning Plus ECL Substrate (Perkin Elmer).

641 **TNF- α ELISA**

642 For quantification of TNF- α in serum samples, the Mouse TNF ELISA Kit (BD Biosciences)
643 was used according to the manufacturer's instructions.

644 **RNA isolation, cDNA transcription, and qPCR**

645 The NucleoSpin® RNA Kit (Macherey Nagel) was used to isolate total RNA from tissues or
646 organoids. Subsequently, cDNA synthesis was performed using the Script cDNA Synthesis Kit
647 (Jena Bioscience). For gene expression measurements, SensiFAST SYBR No-ROX (BioCat)
648 and QuantiTect primers (QIAGEN) were used in a real-time PCR cyclor (Bio-Rad).
649 Normalization was performed with *Gapdh* or *Hprt* as described in the corresponding figure
650 legend.

651 **Bulk RNA sequencing and analysis**

652 For bulk RNA sequencing, QC quality control was performed and samples were sequenced
653 on an Illumina NovaSeq platform (Novogene, Cambridge, UK). STAR (2.7.0d) and feature
654 counts (v1.6.4) were used for mapping to the reference genome (mm10) and quantification,
655 respectively. Differential expression of the groups of samples was performed using DESeq2
656 (1.24.0). Enrichment, clustering, and other analyses were performed using in-house
657 bioinformatic tools and Ingenuity Pathway Analysis (IPA; Qiagen), the Database for

658 Annotation, Visualization and Integrated Discovery (DAVID) analysis tool. Only genes with
659 adjusted p-values less than 0.05 and $\log_2(\text{fold change})$ less or greater than 1 were considered.

660 **Availability and analysis of transcriptomic datasets**

661 Transcriptomic data of the IBDome cohort will be made available to the scientific community
662 upon acceptance of the manuscript. The publicly available datasets used in this study are
663 published under the accession codes: E-MTAB-9850 [28] and GSE6731.[29] The
664 corresponding raw expression values were log-transformed. Microsoft Excel 2019 was used
665 for data sorting and comparison, while GraphPad Prism 9 was used for graphical illustrations.

666 **Statistical analysis**

667 GraphPad Prism 9 software was used for statistical analysis and graphing. As described in the
668 corresponding figure legends, significance analysis was performed using Mann-Whitney test,
669 Student's t-test or one-way ANOVA. P values below 0.05 (*), 0.01 (**), and 0.001 (***) were
670 considered significant. All data are shown as mean \pm SD. Three independent replicates were
671 used in most experiments.

672 **REFERENCES**

- 673 1 Li YM, Xu M, Lai MT, et al. Photoactivated gamma-secretase inhibitors directed to the
674 active site covalently label presenilin 1. *Nature* 2000;405(6787):689–94.
- 675 2 Strooper B de, Saftig P, Craessaerts K, et al. Deficiency of presenilin-1 inhibits the normal
676 cleavage of amyloid precursor protein. *Nature* 1998;391(6665):387–90.
- 677 3 Güner G, Lichtenthaler SF. The substrate repertoire of γ -secretase/presenilin. *Semin Cell*
678 *Dev Biol* 2020;105:27–42.
- 679 4 Duggan SP, McCarthy JV. Beyond γ -secretase activity: The multifunctional nature of
680 presenilins in cell signalling pathways. *Cell Signal* 2016;28(1):1–11.
- 681 5 Lanoiselée H-M, Nicolas G, Wallon D, et al. APP, PSEN1, and PSEN2 mutations in early-
682 onset Alzheimer disease: A genetic screening study of familial and sporadic cases. *PLoS*
683 *Med* 2017;14(3):e1002270.
- 684 6 Sannerud R, Esselens C, Ejsmont P, et al. Restricted Location of PSEN2/ γ -Secretase
685 Determines Substrate Specificity and Generates an Intracellular A β Pool. *Cell*
686 2016;166(1):193–208.
- 687 7 Meckler X, Checler F. Presenilin 1 and Presenilin 2 Target γ -Secretase Complexes to
688 Distinct Cellular Compartments. *J Biol Chem* 2016;291(24):12821–37.
- 689 8 Serneels L, van Biervliet J, Craessaerts K, et al. gamma-Secretase heterogeneity in the
690 Aph1 subunit: relevance for Alzheimer's disease. *Science* 2009;324(5927):639–42.
- 691 9 Shen J, Bronson RT, Chen DF, et al. Skeletal and CNS defects in Presenilin-1-deficient
692 mice. *Cell* 1997;89(4):629–39.
- 693 10 Zhang B, Wang HE, Bai Y-M, et al. Inflammatory bowel disease is associated with higher
694 dementia risk: a nationwide longitudinal study. *Gut* 2021;70(1):85–91.
- 695 11 Kim GH, Lee YC, Kim TJ, et al. Risk of Neurodegenerative Diseases in Patients with
696 Inflammatory Bowel Disease: A Nationwide Population-based Cohort Study. *J Crohns*
697 *Colitis* 2022;16(3):436–43.
- 698 12 Sohrabi M, Pecoraro HL, Combs CK. Gut Inflammation Induced by Dextran Sulfate
699 Sodium Exacerbates Amyloid- β Plaque Deposition in the AppNL-G-F Mouse Model of
700 Alzheimer's Disease. *J Alzheimers Dis* 2021;79(3):1235–55.
- 701 13 Jang S-E, Lim S-M, Jeong J-J, et al. Gastrointestinal inflammation by gut microbiota
702 disturbance induces memory impairment in mice. *Mucosal Immunol* 2018;11(2):369–79.
- 703 14 Baulies A, Angelis N, Li VSW. Hallmarks of intestinal stem cells. *Development*
704 2020;147(15).
- 705 15 Hartman C, Eliakim R, Shamir R. Nutritional status and nutritional therapy in inflammatory
706 bowel diseases. *World J Gastroenterol* 2009;15(21):2570–78.
- 707 16 Lanfranchi GA, Brignola C, Campieri M, et al. Assessment of nutritional status in Crohn's
708 disease in remission or low activity. *Hepatogastroenterology* 1984;31(3):129–32.
- 709 17 Goh J, O'Morain CA. Review article: nutrition and adult inflammatory bowel disease.
710 *Aliment Pharmacol Ther* 2003;17(3):307–20.
- 711 18 Donnellan CF, Yann LH, Lal S. Nutritional management of Crohn's disease. *Therap Adv*
712 *Gastroenterol* 2013;6(3):231–42.
- 713 19 Becker C, Neurath MF, Wirtz S. The Intestinal Microbiota in Inflammatory Bowel Disease.
714 *ILAR J* 2015;56(2):192–204.
- 715 20 Levitan D, Greenwald I. Facilitation of lin-12-mediated signalling by sel-12, a
716 Caenorhabditis elegans S182 Alzheimer's disease gene. *Nature* 1995;377(6547):351–
717 54.
- 718 21 Annaert WG, Levesque L, Craessaerts K, et al. Presenilin 1 controls gamma-secretase
719 processing of amyloid precursor protein in pre-golgi compartments of hippocampal
720 neurons. *J Cell Biol* 1999;147(2):277–94.

- 721 22 Struhl G, Greenwald I. Presenilin is required for activity and nuclear access of Notch in
722 Drosophila. *Nature* 1999;398(6727):522–25.
- 723 23 Zhang Z, Hartmann H, Do VM, et al. Destabilization of beta-catenin by mutations in
724 presenilin-1 potentiates neuronal apoptosis. *Nature* 1998;395(6703):698–702.
- 725 24 Murayama M, Tanaka S, Palacino J, et al. Direct association of presenilin-1 with beta-
726 catenin. *FEBS Lett* 1998;433(1-2):73–77.
- 727 25 Yu G, Chen F, Levesque G, et al. The presenilin 1 protein is a component of a high
728 molecular weight intracellular complex that contains beta-catenin. *J Biol Chem*
729 1998;273(26):16470–75.
- 730 26 Kang DE, Soriano S, Frosch MP, et al. Presenilin 1 facilitates the constitutive turnover of
731 beta-catenin: differential activity of Alzheimer's disease-linked PS1 mutants in the beta-
732 catenin-signaling pathway. *J Neurosci* 1999;19(11):4229–37.
- 733 27 Bagaria J, Bagyinszky E, An SSA. Genetics, Functions, and Clinical Impact of Presenilin-
734 1 (PSEN1) Gene. *Int J Mol Sci* 2022;23(18).
- 735 28 Patankar JV, Müller TM, Kantham S, et al. E-type prostanoid receptor 4 drives resolution
736 of intestinal inflammation by blocking epithelial necroptosis. *Nat Cell Biol* 2021;23(7):796–
737 807.
- 738 29 Wu F, Dassopoulos T, Cope L, et al. Genome-wide gene expression differences in
739 Crohn's disease and ulcerative colitis from endoscopic pinch biopsies: insights into
740 distinctive pathogenesis. *Inflamm Bowel Dis* 2007;13(7):807–21.
- 741 30 Yu H, Saura CA, Choi SY, et al. APP processing and synaptic plasticity in presenilin-1
742 conditional knockout mice. *Neuron* 2001;31(5):713–26.
- 743 31 Herreman A, Hartmann D, Annaert W, et al. Presenilin 2 deficiency causes a mild
744 pulmonary phenotype and no changes in amyloid precursor protein processing but
745 enhances the embryonic lethal phenotype of presenilin 1 deficiency. *Proc Natl Acad Sci*
746 *U S A* 1999;96(21):11872–77.
- 747 32 Becker C, Fantini MC, Neurath MF. High resolution colonoscopy in live mice. *Nat Protoc*
748 2006;1(6):2900–04.
- 749 33 Martini E, Krug SM, Siegmund B, et al. Mend Your Fences: The Epithelial Barrier and its
750 Relationship With Mucosal Immunity in Inflammatory Bowel Disease. *Cellular and*
751 *Molecular Gastroenterology and Hepatology* 2017;4(1):33–46.
752 <https://www.sciencedirect.com/science/article/pii/S2352345X1730053X>.
- 753 34 Bardenbacher M, Ruder B, Britzen-Laurent N, et al. Investigating Intestinal Barrier
754 Breakdown in Living Organoids. *J Vis Exp* 2020(157).
- 755 35 Landy J, Ronde E, English N, et al. Tight junctions in inflammatory bowel diseases and
756 inflammatory bowel disease associated colorectal cancer. *World J Gastroenterol*
757 2016;22(11):3117–26.
- 758 36 Kucharzik T, Walsh SV, Chen J, et al. Neutrophil transmigration in inflammatory bowel
759 disease is associated with differential expression of epithelial intercellular junction
760 proteins. *Am J Pathol* 2001;159(6):2001–09.
- 761 37 Mehta S, Nijhuis A, Kumagai T, et al. Defects in the adherens junction complex (E-
762 cadherin/ β -catenin) in inflammatory bowel disease. *Cell and Tissue Research*
763 2015;360(3):749–60.
- 764 38 Tang H-N, Tang C-Y, Man X-F, et al. Plasticity of adipose tissue in response to fasting
765 and refeeding in male mice. *Nutr Metab (Lond)* 2017;14:3.
- 766 39 Soayfane Z, Tercé F, Cantiello M, et al. Exposure to dietary lipid leads to rapid production
767 of cytosolic lipid droplets near the brush border membrane. *Nutr Metab (Lond)*
768 2016;13(1):48.
- 769 40 Strooper B de, Annaert W, Cupers P, et al. A presenilin-1-dependent gamma-secretase-
770 like protease mediates release of Notch intracellular domain. *Nature*
771 1999;398(6727):518–22.

- 772 41 Reyes Gamez-Belmonte, Mousumi Mahapatro, Lena Erkert, et al. Epithelial presenilin-1
773 drives colorectal tumour growth by controlling EGFR-COX2 signalling. *Gut*
774 2023;72(6):1155.
- 775 42 Aziz M, Ishihara S, Ansary MU, et al. Crosstalk between TLR5 and Notch1 signaling in
776 epithelial cells during intestinal inflammation. *Int J Mol Med* 2013;32(5):1051–62.
- 777 43 Shinoda M, Shin-Ya M, Naito Y, et al. Early-stage blocking of Notch signaling inhibits the
778 depletion of goblet cells in dextran sodium sulfate-induced colitis in mice. *J Gastroenterol*
779 2010;45(6):608–17.
- 780 44 Obata Y, Takahashi D, Ebisawa M, et al. Epithelial cell-intrinsic Notch signaling plays an
781 essential role in the maintenance of gut immune homeostasis. *J Immunol*
782 2012;188(5):2427–36.
- 783 45 Mathern DR, Laitman LE, Hovhannisyanyan Z, et al. Mouse and human Notch-1 regulate
784 mucosal immune responses. *Mucosal Immunol* 2014;7(4):995–1005.
- 785 46 Okamoto R, Tsuchiya K, Nemoto Y, et al. Requirement of Notch activation during
786 regeneration of the intestinal epithelia. *Am J Physiol Gastrointest Liver Physiol*
787 2009;296(1):G23-35.
- 788 47 Zheng X, Tsuchiya K, Okamoto R, et al. Suppression of hath1 gene expression directly
789 regulated by hes1 via notch signaling is associated with goblet cell depletion in ulcerative
790 colitis. *Inflamm Bowel Dis* 2011;17(11):2251–60.
- 791 48 Dahan S, Rabinowitz KM, Martin AP, et al. Notch-1 signaling regulates intestinal epithelial
792 barrier function, through interaction with CD4+ T cells, in mice and humans.
793 *Gastroenterology* 2011;140(2):550–59.
- 794 49 Ghorbaninejad M, Heydari R, Mohammadi P, et al. Contribution of NOTCH signaling
795 pathway along with TNF- α in the intestinal inflammation of ulcerative colitis. *Gastroenterol*
796 *Hepatol Bed Bench* 2019;12(Suppl1):S80-S86.
- 797 50 Collins M, Michot J-M, Bellanger C, et al. Notch inhibitors induce diarrhea, hypercrinia and
798 secretory cell metaplasia in the human colon. *EXCLI J* 2021;20:819–27.
- 799 51 Pant S, Jones SF, Kurkjian CD, et al. A first-in-human phase I study of the oral Notch
800 inhibitor, LY900009, in patients with advanced cancer. *Eur J Cancer* 2016;56:1–9.
- 801 52 Massard C, Azaro A, Soria J-C, et al. First-in-human study of LY3039478, an oral Notch
802 signaling inhibitor in advanced or metastatic cancer. *Ann Oncol* 2018;29(9):1911–17.
- 803 53 Messersmith WA, Shapiro GI, Cleary JM, et al. A Phase I, dose-finding study in patients
804 with advanced solid malignancies of the oral γ -secretase inhibitor PF-03084014. *Clin*
805 *Cancer Res* 2015;21(1):60–67.
- 806 54 Coric V, van Dyck CH, Salloway S, et al. Safety and tolerability of the γ -secretase inhibitor
807 avagacestat in a phase 2 study of mild to moderate Alzheimer disease. *Arch Neurol*
808 2012;69(11):1430–40.
- 809 55 Sancho R, Cremona CA, Behrens A. Stem cell and progenitor fate in the mammalian
810 intestine: Notch and lateral inhibition in homeostasis and disease. *EMBO Rep*
811 2015;16(5):571–81.
- 812 56 Madara JL, Trier JS. Structure and permeability of goblet cell tight junctions in rat small
813 intestine. *J Membr Biol* 1982;66(2):145–57.
- 814 57 Riccio O, van Gijn ME, Bezdek AC, et al. Loss of intestinal crypt progenitor cells owing to
815 inactivation of both Notch1 and Notch2 is accompanied by derepression of CDK inhibitors
816 p27Kip1 and p57Kip2. *EMBO Rep* 2008;9(4):377–83.
- 817 58 Pellegrinet L, Rodilla V, Liu Z, et al. Dll1- and dll4-mediated notch signaling are required
818 for homeostasis of intestinal stem cells. *Gastroenterology* 2011;140(4):1230-1240.e1-7.
- 819 59 Ueo T, Imayoshi I, Kobayashi T, et al. The role of Hes genes in intestinal development,
820 homeostasis and tumor formation. *Development* 2012;139(6):1071–82.
- 821 60 Tsai Y-H, VanDussen KL, Sawey ET, et al. ADAM10 regulates Notch function in intestinal
822 stem cells of mice. *Gastroenterology* 2014;147(4):822-834.e13.

- 823 61 Balestrieri P, Ribolsi M, Guarino MPL, et al. Nutritional Aspects in Inflammatory Bowel
824 Diseases. *Nutrients* 2020;12(2).
- 825 62 Jansen I, Prager M, Valentini L, et al. Inflammation-driven malnutrition: a new screening
826 tool predicts outcome in Crohn's disease. *Br J Nutr* 2016;116(6):1061–67.
- 827 63 Takaoka A, Sasaki M, Nakanishi N, et al. Nutritional Screening and Clinical Outcome in
828 Hospitalized Patients with Crohn's Disease. *Ann Nutr Metab* 2017;71(3-4):266–72.
- 829 64 McGovern DPB, Kugathasan S, Cho JH. Genetics of Inflammatory Bowel Diseases.
830 *Gastroenterology* 2015;149(5):1163-1176.e2.
- 831 65 Jostins L, Ripke S, Weersma RK, et al. Host-microbe interactions have shaped the genetic
832 architecture of inflammatory bowel disease. *Nature* 2012;491(7422):119–24.
- 833 66 Maesako M, Horlacher J, Zoltowska KM, et al. Pathogenic PS1 phosphorylation at
834 Ser367. *Elife* 2017;6.
- 835 67 Faul F, Erdfelder E, Lang A-G, et al. G*Power 3: a flexible statistical power analysis
836 program for the social, behavioral, and biomedical sciences. *Behav Res Methods*
837 2007;39(2):175–91.
- 838 68 Sato T, Vries RG, Snippert HJ, et al. Single Lgr5 stem cells build crypt-villus structures in
839 vitro without a mesenchymal niche. *Nature* 2009;459(7244):262–65.
- 840 69 Johansson MEV, Hansson GC. Preservation of mucus in histological sections,
841 immunostaining of mucins in fixed tissue, and localization of bacteria with FISH. *Methods*
842 *Mol Biol* 2012;842:229–35.
- 843

844 **ACKNOWLEDGEMENTS**

845 This work was funded by the DFG project TRR241 (A03, B05, C04 and Z03), CRC1181 (C05),
846 and individual grants under project numbers 418055832 and 510624836. The Interdisciplinary
847 Center for Clinical Research (IZKF: J68, A76, J96, A93) also supported this project.

848 Parts of the results of this study are subject of the doctoral thesis of LE.

849 **AUTHOR CONTRIBUTIONS**

850 Study concept, design, literature search, experiments, analysis, interpretation of data, critical
851 revision of the manuscript, manuscript drafting: LE, RGB, CB. Experimentation and analysis:
852 LE, RGB, MK, LSc, JVP, MGA, LB, CP, ST. Material support: MM, JS, LSe, BDS, AAK.
853 Intellectual contributions during manuscript editing, acquisition of funds and supervision: MFN,
854 SW, CB.

855 **COMPETING INTERESTS STATEMENT**

856 The authors declare no conflicting financial interests.

857 **FIGURE LEGENDS**

858 **Fig. 1: Psen1 is expressed in the intestine and is differentially regulated during intestinal**
859 **inflammation.**

860 **(A)** KEGG analysis of RNA sequencing data from DSS-treated mouse whole colon tissue
861 compared to healthy mouse colons (n = 3/group). **(B)** *Psen1* counts in the colon of DSS-treated
862 mice at different stages of inflammation with body weight change (%) of the mice, analyzed
863 from a publicly available dataset (n = 2-3/group).[28] **(C)** Western blotting for PSEN1 in colonic
864 tissue lysates from healthy and DSS-treated mice, with measurement of PSEN1 expression,
865 normalized to β -actin (n = 7-8/group). **(D)** Representative immunofluorescence images for
866 *Psen1* (red) and E-Cadherin (green) in the ileum and colon of healthy and severely inflamed
867 DSS-treated mice (scale bar 100 μ m) (representative of 3 independent experiments). **(E)**
868 Normalized Log₂ expression levels of *PSEN1* in healthy (n= 4), Ulcerative colitis (UC) (n= 13)
869 and Crohn's disease (CD) (n= 19) patients analyzed from a publicly available dataset.[29] **(F)**
870 *PSEN1* normalized counts in the colon of healthy (n = 22), Ulcerative colitis (n = 44), and
871 Crohn's disease (n = 41) patients. **(G)** Relative *PSEN1* expression levels in different disease
872 stages of UC and CD patients (n = 5/group). **(H)** Linear regression analysis of *PSEN1* in colonic
873 samples of healthy versus UC patients in correlation with the histopathological score of colitis
874 (n = 60). **(I)** Representative immunofluorescence images of PSEN1 in healthy (n = 4), UC (n =
875 6) and CD patients (n = 4) (scale bar 50 μ m) with analysis of the *Psen1*⁺ area (normalized to
876 Hoechst). Overall, data are expressed as mean \pm SD. *, **, and *** indicate p < 0.05, p < 0.01,
877 and p < 0.001 respectively, by one-way ANOVA (B, E, G, H) Mann-Whitney test (C) or
878 Wilcoxon rank-sum test (F).

879 **Fig. 2: Inducible presenilin double-knockout mice spontaneously develop colitis.**

880 **(A)** Schematic of intraperitoneal (i.p.) injection of tamoxifen in control (*Psen2*^{-/-} *Psen1*^{fl/fl}) and
881 inducible *Psen1/2* double knockout (iDKO; *Psen2*^{-/-} *Psen1*^{i Δ IEC}) mice. **(B)** Daily weight
882 measurements of tamoxifen-injected control and iDKO mice. Weight is expressed as
883 percentage of initial weight (control: n = 5; iDKO: n = 7). **(C)** Representative endoscopic images

884 and murine endoscopic index of colitis severity (MEICS) scoring in control and iDKO mice
885 (control: n = 13; iDKO: n = 15). **(D)** Measurement of colon length in the different mouse strains
886 (control: n = 11; iDKO: n = 9). **(E)** Representative H&E images of ileum and proximal and distal
887 colon from control and iDKO mice (scale bar 250 μ m) with histology scoring of duodenum,
888 jejunum, ileum, proximal and distal colon. Yellow arrows indicate cell death, and black arrows
889 indicate mucus accumulation (representative of 3 independent experiments). **(F)** qPCR
890 analysis of several inflammatory cytokines (normalized to *Gapdh*) from ileum and colon of the
891 shown mice (control: n = 8; iDKO: n = 11). **(G)** Representative IF images for MPO (neutrophils)
892 and F4/80 (macrophages) in the ileum and colon of the different genotypes (scale bar 100 μ m)
893 (control: n = 5-6; iDKO: n = 7-10) with analysis of the MPO⁺ cells (per high power field (HPF))
894 and F4/80⁺ area (normalized to Hoechst). Overall, data are expressed as mean \pm SD. *, **,
895 and *** indicate p < 0.05, p < 0.01 and p < 0.001, respectively, by one-way ANOVA (B) and
896 Mann-Whitney test (C, D, F, G).

897 **Fig. 3: Presenilins are key to intestinal barrier function.**

898 **(A)** Measurement of FITC-dextran in the serum of tamoxifen-injected control (*Psen2*^{-/-} *Psen1*^{fl/fl})
899 and inducible *Psen1/2* double knockout (iDKO; *Psen2*^{-/-} *Psen1* ^{Δ IEC}) mice (control: n = 8; iDKO:
900 n = 11). **(B)** Lucifer yellow uptake in Si organoids with analysis of the mean value of relative
901 intensity increase (scale bar 100 μ m) (representative of 3 independent experiments). Dashed
902 lines indicate the lumen of the organoids. **(C)** Representative IF images for E-Cadherin in the
903 ileum and colon of control and iDKO mice (scale bar 100 μ m) (representative of 3 independent
904 experiments). **(D)** Western blot analysis for Occludin in ileal and colonic tissue extracts from
905 the indicated mice. β -actin was used as a loading control (representative of 3 independent
906 experiments). **(E)** Occludin and *Psen1* protein expression levels in the ileum of control and
907 iDKO mice; control mice were sacrificed on day 8 after the first dose of tamoxifen, iDKO mice
908 were sacrificed on day 5, day 6, day 7, and day 8 after the first dose. β -actin was used as a
909 loading control (1 experiment). **(F)** Representative FISH staining images for Eub338 (white
910 arrows) in the ileum and colon of the indicated mouse strains (scale bar 100 μ m)
911 (representative of 3 independent experiments). **(G)** Tissue plating of mesenteric lymph node

912 (MLN) and liver tissue extracts from the different genotypes cultured under aerobic and
913 anaerobic conditions, including assessment of colony forming units (CFU)/g stool (n =
914 ≥ 7 /group). **(H)** Analysis of TNF- α levels in serum of control and iDKO mice (control: n = 4;
915 iDKO: n = 6). **(I)** qPCR analysis of *Tnf* and *Nos2* in spleen tissue of the different genotypes
916 (control: n = 11; iDKO: n = 7). **(J)** Assessment of serum aspartate aminotransferase (AST) and
917 alanine aminotransferase (ALT) levels (control: n = 18; iDKO: n = 17). Overall, data are
918 expressed as mean \pm SD. *, **, and *** indicate p < 0.05, p < 0.01, and p < 0.001, respectively,
919 by Mann-Whitney test.

920 **Fig. 4: Microbiota depletion improves spontaneous inflammation but not body weight**
921 **loss in inducible presenilin double-knockout mice.**

922 **(A)** Schematic of antibiotic (Ab) treatment in drinking water and i.p. tamoxifen injection in
923 control (Psen2^{-/-} Psen1^{fl/fl}) and inducible Psen1/2 double knockout (iDKO; Psen2^{-/-} Psen1^{i Δ IEC})
924 mice. **(B)** Stool lysates plated on agar plates with corresponding evaluation of CFU/g stool
925 (control: n = 9; iDKO: n = 10). **(C)** Daily weight measurements presented as percentage of
926 initial weight in control and iDKO animals treated with or without antibiotics (n \geq 3/group). **(D)**
927 Representative endoscopic images and MEICS score (n \geq 3/group). **(E)** Representative H&E
928 staining images of ileum and colon sections of the indicated mice and treatments (scale bar
929 250 μ m) (n \geq 3/group). **(F)** Histological scoring of ileal and colonic tissue sections of the
930 different treatment groups indicated (n \geq 3/group). **(G)** qPCR analysis for various inflammatory
931 markers (normalized to *Hprt*) in the ileum and colon of control and iDKO mice treated with and
932 without antibiotics (n \geq 3/group). Overall, data are expressed as mean \pm SD. *, **, and ***
933 indicate p < 0.05, p < 0.01, and p < 0.001, respectively, by Mann-Whitney test (B) or one-way
934 ANOVA (C, D, F).

935 **Fig. 5: Dual presenilin deletion leads to enterocyte loss, malnutrition and death in**
936 **presenilin double knockout mice due to Notch signaling disruption.**

937 **(A)** Volcano plot of RNA sequencing analysis of inducible Psen1/2 double knockout (iDKO;
938 Psen2^{-/-} Psen1^{i Δ IEC}) ileal tissue compared to control littermates (Psen2^{-/-} Psen1^{fl/fl}) (p-adjusted
939 < 0.05; log₂foldchange \pm 1). Green dots represent downregulation, red dots represent

940 upregulation, and gray indicates no gene deregulation (n = 3/group). DEG = differentially
941 expressed genes. **(B)** Selected gene ontology biological process (GO_BP) and KEGG
942 pathways of the described RNAseq dataset (n = 3/group). Red bars indicate upregulation,
943 green bars indicate downregulation. **(C)** Heatmap of RNA sequencing analysis of ileal tissue
944 from control and iDKO mice (n = 3/group) for absorptive enterocyte-specific genes (n =
945 3/group). **(D)** Images of intestinal alkaline phosphatase (IAP; bordeaux; enterocyte marker)
946 staining in the ileum of control and iDKO mice (scale bar 100 μ m) with analysis of IAP+ area
947 normalized to hematoxylin (n = 5-7/group). **(E)** Measurement of serum glucose levels of
948 indicated mice (control: n = 31; iDKO: n = 28). **(F)** Rhodamine 123 uptake and relative
949 measured Rhodamine 123 intensity in the lumen of Si organoids generated from control and
950 iDKO mice treated with 50 ng/ml tamoxifen for 5 days (scale bar 100 μ m) (representative of 3
951 independent experiments). **(G)** Oral glucose tolerance test in control and iDKO mice using 2.5
952 g glucose/kg body weight (control: n = 10; iDKO: n = 6). **(H)** Representative H&E staining
953 images of mesenteric fat and analysis of the area of fat cells from the two mouse strains (scale
954 bar 250 μ m) (control: n = 15; iDKO: n = 8). **(I)** Representative immunofluorescence staining
955 images of HCS LipidTOX in the duodenum of control and iDKO mice with analysis of HCS
956 LipidTOX positive area normalized to Hoechst (scale bar 100 μ m) (control: n = 9; iDKO: n =
957 6). **(J)** Representative images of Periodic Acid-Schiff (PAS) staining on liver tissue samples
958 from control and iDKO mice with analysis of PAS⁺ staining (fold change) (scale bar 100 μ m)
959 (control: n = 17; iDKO: n = 9). **(K)** Analysis of Notch intracellular domain (NICD) protein
960 expression by Western blotting of ileal and colonic tissue extracts from Psen1 ^{Δ IEC}, Psen2^{-/-} and
961 iDKO mice and their respective controls. β -actin was used as a loading control (representative
962 of 3 independent experiments). **(L)** Schematic of the influence of a dual Psen1 and Psen2
963 deletion on intestinal homeostasis. Overall, data are expressed as mean \pm SD. ** and ***
964 indicate p < 0.01, and p < 0.001, respectively, by Mann-Whitney test (D, E, F, H, I, J) or two-
965 way ANOVA (G).

966 **Suppl. Fig. 1: Involvement of genes associated with neurodegeneration and Alzheimer's**
967 **disease in intestinal inflammation.**

968 Heatmaps of RNA sequencing data from DSS-treated mouse whole colon tissue compared to
969 healthy mouse colons showing differentially expressed genes included in the pathways
970 'Pathways of neurodegeneration – multiple diseases' and 'Alzheimer's disease'. *Psen1* is
971 highlighted with a red arrow and *Psen2* with a blue arrow (n = 3/group).

972 **Suppl. Fig. 2: Generation of intestinal epithelial specific *Psen1* deficient mice.**

973 **(A)** Schematic of *Psen1*^{ΔIEC} mouse line generation. **(B)** *Psen1* mRNA expression levels,
974 normalized to *Gapdh*, in the ileum and colon of *Psen1*^{ΔIEC} mice compared to *Psen1*^{fl/fl} mice
975 (*Psen1*^{fl/fl}: n = 10; *Psen1*^{ΔIEC}: n = 10). **(C)** Western blotting for *Psen1* in whole ileal and colonic
976 tissue extracts and in isolated IEC from *Psen1*^{fl/fl} (fl/fl) and *Psen1*^{ΔIEC} (ΔIEC) mice. β-actin was
977 used as a loading control (representative of 3 independent experiments). **(D)** Representative
978 IF images of *Psen1* in the ileum and colon of the indicated mice (scale bar 100 μm)
979 (representative of 3 independent experiments). **(E)** *Psen1* protein expression levels in small
980 intestinal organoids generated from *Psen1*^{fl/fl} (fl/fl) and *Psen1*^{ΔIEC} (ΔIEC) mice. β-actin was
981 used as a loading control (representative of 3 independent experiments). **(F)** *Psen1* mRNA
982 expression, normalized to *Gapdh*, in Si organoids established from the two mouse genotypes
983 (3 independent experiments). **(G)** Histochemical staining images of *Psen1* in paraffin-
984 embedded Si organoids (scale bar 100 μm) (representative of 2 independent experiments).
985 Overall, data are expressed as mean ± SD. *** indicates p < 0.001 by one-way ANOVA (B) or
986 Mann-Whitney test (F).

987 **Suppl. Fig. 3: Absence of *Psen1* alone in IECs does not disrupt intestinal tissue or**
988 **immune homeostasis.**

989 **(A)** Hematoxylin & eosin (H&E) staining images of ileal and colonic sections from *Psen1*^{fl/fl} and
990 *Psen1*^{ΔIEC} mice (scale bar 250 μm) (representative of 4 independent experiments). **(B)** qPCR
991 analysis of various IEC differentiation markers (all normalized to *Gapdh*) in the ileum and colon
992 of *Psen1*^{ΔIEC} mice compared to their control littermates (*Psen1*^{fl/fl}: n = 7; *Psen1*^{ΔIEC}: n = 6). **(C)**
993 Representative IF images of different IEC differentiation markers: Muc2 (goblet cells),
994 Chromogranin A (Chga; enteroendocrine cells), Dcamk11 (tuft cells), Ki67 (proliferation), Olfm4

995 (stem cells), intestinal alkaline phosphatase (IAP; absorptive enterocytes) and lysozyme (Lyz;
996 Paneth cells) in the ileum and colon of the different mouse genotypes (white scale bar 100 μm ;
997 yellow scale bar 250 μm) (representative of 3 independent experiments). **(D)** Analysis of Chga-
998 and Dcamk11-positive cells per high power field (HPF) in the ileum and colon of $\text{Psen1}^{\Delta\text{IEC}}$ mice
999 compared to their littermate controls (3 independent experiments). **(E)** qPCR analysis of
1000 several inflammatory markers in the ileum and colon of $\text{Psen1}^{\text{fl/fl}}$ and $\text{Psen1}^{\Delta\text{IEC}}$ mice ($\text{Psen1}^{\text{fl/fl}}$:
1001 $n = 7$; $\text{Psen1}^{\Delta\text{IEC}}$: $n = 6$). **(F)** Volcano plots of RNAseq data obtained from ileal and colonic
1002 tissue of $\text{Psen1}^{\Delta\text{IEC}}$ mice compared to their control mice. Red dots indicate upregulated genes,
1003 green dots indicate downregulation, while gray dots represent genes that are not differentially
1004 expressed ($n = 3/\text{group}$). **(G)** Western blot analysis of PSEN2 expression in the ileum and
1005 colon of $\text{Psen1}^{\text{fl/fl}}$ (fl/fl) and $\text{Psen1}^{\Delta\text{IEC}}$ (ΔIEC) mice (representative of 3 independent
1006 experiments) with analysis of PSEN2 protein abundance normalized to β -actin. Overall, data
1007 are expressed as mean \pm SD. * and ** indicate $p < 0.05$ and $p < 0.01$, respectively, by one-
1008 way ANOVA (G).

1009 **Suppl. Fig. 4: One allele of Psen2 is sufficient to maintain intestinal homeostasis in**
1010 **heterozygous presenilin double-knockout mice.**

1011 **(A)** Schematic of the generation of conditional presenilin double-knockout mice. **(B)** Listing of
1012 the Mendelian expected genotypes of the crossing shown in (A) compared to the actual
1013 genotypes obtained. **(C)** Weekly body weight measurements of control mice ($\text{Psen2}^{-/-} \text{Psen1}^{\text{fl/fl}}$)
1014 compared to heterozygous conditional presenilin double-knockout mice ($\text{Psen2}^{+/-} \text{Psen1}^{\Delta\text{IEC}}$)
1015 ($n = 4/\text{group}$). **(D)** Representative endoscopic images of control and $\text{Psen2}^{+/-} \text{Psen1}^{\Delta\text{IEC}}$ mice
1016 with corresponding MEICS scores (control: $n = 10$; $\text{Psen2}^{+/-} \text{Psen1}^{\Delta\text{IEC}}$: $n = 9$). **(E)**
1017 Representative H&E images of the ileum, proximal and distal colon from control and $\text{Psen2}^{+/-}$
1018 $\text{Psen1}^{\Delta\text{IEC}}$ mice (scale bar 250 μm) (representative of 5 independent experiments). **(F)**
1019 Representative IF images for *Olfm4* (stem cells) and *Muc2* (goblet cells) in the ileum of control
1020 and $\text{Psen2}^{+/-} \text{Psen1}^{\Delta\text{IEC}}$ mice (scale bar 100 μm) (representative of 3 independent
1021 experiments). **(G)** qPCR analysis of various IEC differentiation markers (all normalized to
1022 *Gapdh*) of ileal and colonic tissues from the indicated mouse strains (control: $n = 13$; $\text{Psen2}^{+/-}$

1023 Psen1^{ΔIEC}: n = 7). **(H)** Western blot analysis for Notch intracellular domain (NICD) in the ileum
1024 and colon of the different genotypes. β-actin was used as a loading control (representative of
1025 3 independent experiments). Overall, data are expressed as mean ± SD.

1026 **Suppl. Fig. 5: Absence of Psen2 alone does not disrupt intestinal tissue or immune**
1027 **homeostasis.**

1028 **(A)** Western blot for Psen2 expression analyzed in protein extracts of ileum and colon from
1029 Psen2^{+/+} and Psen2^{-/-} mice (representative of 3 independent experiments). **(B)** Hematoxylin &
1030 eosin (H&E) staining images of ileal and colonic sections from Psen2^{+/+} and Psen2^{-/-} mice
1031 (scale bar 250 μm) (representative of 4 independent experiments). **(C)** qPCR analysis of
1032 various IEC differentiation markers (all normalized to *Gapdh*) in the ileum and colon of Psen2^{-/-}
1033 mice compared to their control littermates (Psen2^{+/+}: n = 7; Psen2^{-/-}: n = 9). **(D)** Representative
1034 IF images of different IEC differentiation markers: Muc2 (goblet cells), Chromogranin A (Chga;
1035 enteroendocrine cells), Dcamk11 (tuft cells), Ki67 (proliferation), Olfm4 (stem cells), intestinal
1036 alkaline phosphatase (IAP; absorptive enterocytes) and lysozyme (Lyz; Paneth cells) in the
1037 ileum and colon of the different mouse genotypes (white scale bar 100 μm; yellow scale bar
1038 250 μm) (representative of 3 independent experiments). **(E)** Analysis of Chga- and Dcamk11-
1039 positive cells per high power field (HPF) in the ileum and colon of Psen2^{-/-} mice compared to
1040 their littermate controls (3 independent experiments). **(F)** qPCR analysis of several
1041 inflammatory markers in the ileum and colon of Psen2^{+/+} and Psen2^{-/-} mice (Psen2^{+/+}: n = 7;
1042 Psen2^{-/-}: n = 9). **(G)** Volcano plots of RNAseq data obtained from ileal tissue of Psen2^{-/-} mice
1043 compared to their control mice. Red dots indicate upregulated genes, green dots indicate
1044 downregulation, while gray dots represent not differentially expressed genes (n = 3/group).
1045 Overall, data are expressed as mean ± SD.

1046 **Suppl. Fig. 6: Inducible presenilin double-knockout mice lack Psen1 and Psen2 in the**
1047 **IECs.**

1048 **(A)** Schematic of the generation of inducible Psen1/2 double knockout mice. **(B)** *Psen1* mRNA
1049 expression levels in ileal and colonic tissue samples from control (Psen2^{-/-} Psen1^{fl/fl}) and

1050 inducible *Psen1/2* double knockout (iDKO; *Psen2*^{-/-} *Psen1*^{ΔIEC}) mice. *Gapdh* was used for
1051 normalization (control: n = 5; iDKO: n = 7). **(C)** *Psen1* and *Psen2* protein levels analyzed by
1052 Western blot in the ileum and colon of the indicated mouse strains. β -actin was used as a
1053 loading control (representative of 3 independent experiments). **(D)** Representative IF images
1054 for *Psen1* in ileum and colon of control and iDKO mice (scale bar 100 μ m) (representative of
1055 3 independent experiments). **(E)** qPCR analysis for *Psen1* in Si organoids generated from the
1056 indicated genotypes (3 independent experiments). **(F)** Western blot analysis of Si organoid
1057 protein lysates from the different mouse strains (representative of 3 independent experiments).
1058 Overall, data are expressed as mean \pm SD. *** indicates $p < 0.001$ by one-way ANOVA (B) or
1059 Mann-Whitney test (E).

1060 **Suppl. Fig. 7: IECs lacking *Psen1* and *Psen2* have a pro-inflammatory signature and an**
1061 **impaired differentiation.**

1062 **(A)** Schematic of treatment with 50 ng/ml tamoxifen in control (*Psen2*^{-/-} *Psen1*^{fl/fl}) and inducible
1063 *Psen1/2* double knockout (iDKO; *Psen2*^{-/-} *Psen1*^{ΔIEC}) small intestinal organoids for 5 days. **(B)**
1064 Representative bright field images of Si organoids generated from control and iDKO mice
1065 stimulated as depicted in (A) (scale bar 100 μ m) (representative of 3 independent experiments)
1066 with organoid size measurement. **(C)** Representative IF staining images of occludin in Si
1067 organoids generated from control and iDKO mice (scale bar 100 μ m) (representative of 3
1068 independent experiments). **(D)** mRNA expression levels of various IEC differentiation markers
1069 in small intestinal organoids from the two different mouse strains. *Gapdh* was used for
1070 normalization (3 independent experiments). **(E)** Representative IF staining images for different
1071 IEC differentiation markers: *Olfm4* (stem cells), *ULEX* (goblet cells), *Chga* (Chga;
1072 enteroendocrine cells), *lysozyme* (*Lyz*; Paneth cells), *Dcamk1l* (tuft cells), and *Ki67*
1073 (proliferation) (scale bar 100 μ m) (representative of 3 independent experiments). **(F)** Analysis
1074 of Notch intracellular domain (NICD) protein expression by Western blotting of small intestinal
1075 (Si) organoids established from iDKO and control mice. β -actin was used as a loading control
1076 (representative of 3 independent experiments). Overall, data are expressed as mean \pm SD. **
1077 and *** indicate $p < 0.01$, and $p < 0.001$, respectively, by Mann-Whitney test.

1078 **Suppl. Fig. 8: Psen1 and Psen2 deficiency leads to impaired IEC differentiation.**
1079 **(A)** Selected Ingenuity Pathway Analysis (IPA; Qiagen) for affected diseases and functions in
1080 the RNAseq dataset from ileal tissue of inducible Psen1/2 double knockout (iDKO; Psen2^{-/-}
1081 Psen1^{iΔIEC}) and control (Psen2^{-/-} Psen1^{fl/fl}) mice (n = 3/group). Red bars indicate a positive Z-
1082 score (upregulation), green bars indicate a negative Z-score (downregulation). **(B)** Volcano
1083 plots of RNA sequencing analysis for goblet-, Paneth-, and enteroendocrine-specific genes (n
1084 = 3/group). **(C, D)** Representative staining images for different IEC differentiation markers in
1085 the ileum and colon of the mice: **(C)** Olfm4 (stem cells), Lgr5 (stem cells), Ki67 (proliferation),
1086 **(D)** lysozyme (Lyz; Paneth cells), Muc2 (goblet cells) and Chromogranin A (Chga;
1087 enteroendocrine) (scale bar 100 μm) with analysis of cell type abundance per high power field
1088 (HPF) (n = 5-10/group). Overall, data are expressed as mean ± SD. ** and *** indicate p <
1089 0.01, and p < 0.001, respectively, by Student's t-test (C (Olfm4), D (Lyz)) or Mann-Whitney test
1090 (C (Lgr5, Ki67), D (Muc2, Chga)).

1091 **Suppl. Fig. 9: Presenilins play a crucial role in maintaining tissue homeostasis.**
1092 **(A)** Measurement of serum glucose levels of antibiotic-treated control and iDKO (control: n =
1093 12; iDKO: n = 12). **(B)** Oral glucose tolerance test in control and iDKO mice using 2.5 g
1094 glucose/kg body weight (control: n = 5; iDKO: n = 6). **(C)** Schematic of the role of presenilins
1095 in intestinal homeostasis. Overall, data are expressed as mean ± SD. ** and *** indicate p <
1096 0.01, and p < 0.001, respectively, by Student's t-test (A) or two-way ANOVA (B).

1097 **TABLES**

1098 **Suppl. Tab. 1:** KEGG pathway analysis of ileal samples from iDKO mice compared to control
 1099 mice on day 8 after the first tamoxifen injection (p-adjusted < 0.05; log₂foldchange ± 1).

Pathways	PValue	FDR
Metabolic pathways	1,20E-31	2,99E-29
Carbon metabolism	8,76E-12	1,09E-09
Peroxisome	1,35E-10	1,12E-08
Fat digestion and absorption	9,50E-08	5,91E-06
Biosynthesis of amino acids	2,24E-07	1,12E-05
PPAR signaling pathway	4,15E-06	1,54E-04
Glycerophospholipid metabolism	4,34E-06	1,54E-04
Biosynthesis of cofactors	7,62E-06	2,37E-04
Glycolysis / Gluconeogenesis	1,17E-05	3,12E-04
Citrate cycle (TCA cycle)	1,25E-05	3,12E-04
Bladder cancer	2,49E-05	5,63E-04
Maturity onset diabetes of the young	3,36E-05	6,79E-04
Mineral absorption	3,55E-05	6,79E-04
Ascorbate and aldarate metabolism	4,13E-05	7,34E-04
Bile secretion	5,38E-05	8,93E-04
Mucin type O-glycan biosynthesis	6,37E-05	9,32E-04
Glyoxylate and dicarboxylate metabolism	6,37E-05	9,32E-04
Fatty acid degradation	6,87E-05	9,50E-04
Pyruvate metabolism	7,31E-05	9,50E-04
Retinol metabolism	7,63E-05	9,50E-04
Proximal tubule bicarbonate reclamation	8,89E-05	0,00105362
Vitamin digestion and absorption	2,38E-04	0,00268898

Sulfur metabolism	2,61E-04	0,00283071
Pentose phosphate pathway	4,10E-04	0,00425848
Parathyroid hormone synthesis, secretion and action	5,81E-04	0,00578856
Pancreatic secretion	6,79E-04	0,00650625
Cellular senescence	8,64E-04	0,00796786
Arginine biosynthesis	0,00104523	0,00889548
Pentose and glucuronate interconversions	0,00108395	0,00889548
Fructose and mannose metabolism	0,00108395	0,00889548
Glycerolipid metabolism	0,00112913	0,00889548
beta-Alanine metabolism	0,00114319	0,00889548
Small cell lung cancer	0,00132942	0,01003105
Nitrogen metabolism	0,00139984	0,01025175
Human cytomegalovirus infection	0,00153482	0,01074698
Prostate cancer	0,00155378	0,01074698
Phosphatidylinositol signaling system	0,00215034	0,01376125
Tryptophan metabolism	0,00215538	0,01376125
ABC transporters	0,00215538	0,01376125
Folate biosynthesis	0,00235303	0,01464759
Glutathione metabolism	0,00255794	0,01527716
Gastric cancer	0,00257687	0,01527716
Steroid hormone biosynthesis	0,00297108	0,01720463
Arginine and proline metabolism	0,00330297	0,01869179
Chemical carcinogenesis - receptor activation	0,00343158	0,01898805
Central carbon metabolism in cancer	0,00360391	0,01950814
Cholesterol metabolism	0,00384428	0,02036652
Arachidonic acid metabolism	0,00418117	0,02168982

2-Oxocarboxylic acid metabolism	0,0048408	0,02459915
Calcium signaling pathway	0,00531401	0,02609483
PI3K-Akt signaling pathway	0,00534472	0,02609483
Drug metabolism - other enzymes	0,00548116	0,02624635
Valine, leucine and isoleucine degradation	0,00592837	0,02718675
Inositol phosphate metabolism	0,00597724	0,02718675
Fatty acid metabolism	0,0060051	0,02718675
alpha-Linolenic acid metabolism	0,00643233	0,02860089
p53 signaling pathway	0,00700645	0,03040931
NOD-like receptor signaling pathway	0,00708329	0,03040931
Alanine, aspartate and glutamate metabolism	0,00746731	0,03151456
EGFR tyrosine kinase inhibitor resistance	0,00797674	0,03310346
Kaposi sarcoma-associated herpesvirus infection	0,00854082	0,03450642
Histidine metabolism	0,00859196	0,03450642
Glycine, serine and threonine metabolism	0,00928812	0,0367102
Linoleic acid metabolism	0,0099596	0,03874907
Insulin secretion	0,01022729	0,03917838
Human T-cell leukemia virus 1 infection	0,01051735	0,03967909
Butanoate metabolism	0,01125943	0,04184476
Nicotinate and nicotinamide metabolism	0,01143596	0,0418758
Hepatitis C	0,01236444	0,04461951
Ras signaling pathway	0,01283799	0,04500141
Glucagon signaling pathway	0,01295917	0,04500141
TNF signaling pathway	0,01301246	0,04500141
Hematopoietic cell lineage	0,01437238	0,04902359

1101 **Suppl. Tab. 2:** Gene ontology biological process pathway analysis of ileal samples from iDKO
 1102 mice compared to control mice on day 8 after the first tamoxifen injection (p-adjusted < 0.05;
 1103 log₂foldchange ± 1).

Pathways	PValue	FDR
lipid metabolic process	5,70E-27	4,00E-23
transmembrane transport	1,12E-14	3,92E-11
fatty acid metabolic process	2,38E-10	4,55E-07
lipid transport	2,59E-10	4,55E-07
cholesterol homeostasis	1,64E-09	2,31E-06
gluconeogenesis	3,84E-08	4,49E-05
ion transport	6,98E-08	7,00E-05
immune system process	2,06E-07	1,80E-04
inflammatory response	2,31E-07	1,80E-04
positive regulation of peptidyl-tyrosine phosphorylation	8,31E-07	5,83E-04
sodium ion transport	1,30E-06	8,28E-04
receptor-mediated endocytosis	1,80E-06	0,00105003
response to nutrient	2,06E-06	0,00111205
very long-chain fatty acid metabolic process	3,90E-06	0,00183662
response to xenobiotic stimulus	3,93E-06	0,00183662
steroid metabolic process	5,03E-06	0,00220575
cell migration	6,14E-06	0,00253413
epidermal growth factor receptor signaling pathway	7,31E-06	0,00274161
fatty acid beta-oxidation	7,59E-06	0,00274161
phosphorylation	7,81E-06	0,00274161
aging	1,13E-05	0,00376145
response to sodium phosphate	2,35E-05	0,0074971
response to oxidative stress	2,99E-05	0,0091168

defense response to virus	3,96E-05	0,01159348
carbohydrate metabolic process	4,49E-05	0,0123596
cell surface receptor signaling pathway	4,62E-05	0,0123596
positive regulation of apoptotic process	4,76E-05	0,0123596
positive regulation of cellular respiration	6,86E-05	0,01719422
positive regulation of MAP kinase activity	7,28E-05	0,01761366
wound healing	7,83E-05	0,01832357
cholesterol metabolic process	8,42E-05	0,01905063
positive regulation of cell migration	8,96E-05	0,0196403
ERBB2-EGFR signaling pathway	1,03E-04	0,02185839
glucose metabolic process	1,11E-04	0,0228521
triglyceride biosynthetic process	1,16E-04	0,02322057
triglyceride homeostasis	1,25E-04	0,02410963
amino acid transport	1,27E-04	0,02410963
negative regulation of viral genome replication	1,41E-04	0,0259911
regulation of cell shape	1,56E-04	0,02808965
intestinal absorption	1,60E-04	0,02815363
negative regulation of inflammatory response	1,90E-04	0,03216618
phylloquinone catabolic process	1,93E-04	0,03216618
pyruvate metabolic process	2,13E-04	0,0347233
actin filament organization	2,44E-04	0,03888719
tricarboxylic acid cycle	2,51E-04	0,0392158
negative regulation of cysteine-type endopeptidase activity		
involved in apoptotic process	2,62E-04	0,03996263
ureteric bud development	2,87E-04	0,04283933
metal ion transport	2,93E-04	0,04283933
axon guidance	3,43E-04	0,04875527

one-carbon metabolic process

3,47E-04

0,04875527

1104

1105 **Suppl. Tab. 3:** Ingenuity Pathway Analysis for diseases and functions of ileal samples from
 1106 iDKO mice compared to control mice on day 8 after the first tamoxifen injection (p-adjusted <
 1107 0.05; log₂foldchange ± 1).

Diseases or Functions Annotation	p-value	Activation z-score
Non-hematological solid tumor	2,54E-62	3,144
Epithelial neoplasm	6,50E-62	2,712
Nonhematologic malignant neoplasm	1,39E-61	2,466
Tumorigenesis of tissue	4,39E-61	2,565
Non-melanoma solid tumor	8,44E-61	3,739
Carcinoma	2,94E-60	2,775
Abdominal carcinoma	4,91E-54	2,787
Abdominal lesion	3,58E-53	3,647
Digestive organ tumor	1,43E-52	2,302
Adenocarcinoma	6,72E-52	2,534
Formation of solid tumor	9,68E-52	2,930
Abdominal neoplasm	2,74E-51	2,243
Abdominal adenocarcinoma	1,48E-50	2,648
Extrapancreatic malignant tumor	2,69E-50	2,299
Extracranial solid tumor	1,26E-49	2,919
Abdominal cancer	5,94E-49	2,079
Intraabdominal organ tumor	1,10E-48	2,380
Malignant solid tumor	1,23E-48	3,211
Solid tumor	1,25E-48	3,811
Digestive system cancer	2,30E-48	2,083
Cancer	8,37E-48	3,955

Generation of tumor	9,67E-48	3,267
Gastrointestinal tumor	2,79E-45	2,025
Large intestine neoplasm	1,62E-42	2,180
Malignant solid organ tumor	4,83E-41	2,279
Transport of molecule	1,12E-40	-4,012
Malignant neoplasm of large intestine	5,24E-39	2,070
Incidence of tumor	2,75E-34	2,035
Tumorigenesis of epithelial neoplasm	7,89E-34	2,650
Cell movement	1,57E-32	2,068
Migration of cells	4,51E-30	2,133
Synthesis of lipid	7,05E-30	-2,930
Fatty acid metabolism	1,72E-29	-3,385
Development of carcinoma	1,90E-29	2,575
Development of malignant tumor	3,50E-29	2,594
Breast or colorectal cancer	1,92E-23	2,795
Metabolism of terpenoid	9,70E-23	-2,772
Colorectal tumor	2,04E-22	2,180
Liver lesion	8,19E-22	3,555
Colon tumor	2,81E-20	2,382
Hepatobiliary carcinoma	1,99E-19	2,025
Metabolism of membrane lipid derivative	5,67E-19	-3,017
Oxidation of lipid	1,14E-18	-4,637
Steroid metabolism	1,47E-18	-2,343
Genitourinary carcinoma	1,50E-18	2,598
Liver carcinoma	3,60E-18	2,204
Colorectal cancer	4,65E-18	2,070

Liver tumor	2,76E-17	2,112
Proliferation of epithelial cells	9,10E-17	3,543
Organismal death	1,05E-16	3,759
Growth of lesion	1,08E-16	2,300
Growth of tumor	2,29E-16	2,242
Pelvic carcinoma	2,74E-15	2,121
Development of vasculature	3,54E-15	2,538
Growth of epithelial tissue	5,14E-15	2,726
Conversion of lipid	8,70E-15	-2,628
Oxidation of fatty acid	9,34E-15	-4,431
Angiogenesis	3,28E-14	2,523
Vasculogenesis	1,74E-13	2,575
Cell death of liver cells	2,04E-13	2,231
Transport of lipid	2,13E-13	-4,123
Lipolysis	3,14E-13	-2,070
Uptake of lipid	4,29E-13	-2,730
Necrosis of liver	5,30E-13	2,272
Accumulation of lipid	5,47E-13	2,345
Growth of solid tumor	5,78E-13	2,685
Cell death of liver	6,78E-13	2,353
Cell transformation	1,11E-12	2,306
Damage of genitourinary system	1,50E-12	2,158
Cell death of parenchymal cells	2,89E-12	2,310
Neoplasia of cells	3,04E-12	2,375
Infection by RNA virus	3,91E-12	-2,248
Necrosis of liver parenchyma	7,29E-12	2,433
Cell death of hepatocytes	1,47E-11	2,338

Beta-oxidation of fatty acid	1,60E-11	-3,040
Cell movement of tumor cell lines	2,22E-11	3,158
Quantity of metal	2,78E-11	2,781
Cancer of cells	8,13E-11	2,264
Damage of urinary system	9,11E-11	2,448
Invasive cancer	1,23E-10	2,731
Viral Infection	1,36E-10	-2,752
Advanced malignant tumor	1,58E-10	2,719
Metabolism of sterol	1,64E-10	-2,206
Apoptosis of liver cells	1,87E-10	3,268
Damage of kidney	2,02E-10	2,348
Differentiation of epithelial cells	2,70E-10	2,116
Apoptosis of liver	3,21E-10	3,359
Lymphoid cancer	3,89E-10	2,145
Export of molecule	5,18E-10	-2,267
Differentiation of epithelial tissue	6,34E-10	2,006
Familial neurological disorder	7,12E-10	2,058
Quantity of metal ion	7,14E-10	2,841
Conversion of fatty acid	8,50E-10	-2,750
Flux of lipid	9,78E-10	-2,029
Apoptosis of hepatocytes	1,27E-09	2,939
Urination disorder	1,39E-09	2,210
Quantity of Ca ²⁺	1,42E-09	2,436
Metabolism of xenobiotic	1,77E-09	-3,266
Accumulation of acylglycerol	1,85E-09	2,083

1108

1109 **Suppl. Tab. 4:** Pathoclinical characteristics of IBD patients included in the
1110 immunofluorescence staining analysis (n=14) (NA: not available).

Group	No.	Localization	Histopathology score
healthy	1	Colon	0
healthy	2	Colon	0
healthy	3	Sigmoid colon	0
healthy	4	Ascending colon	0
UC	1	Colon	13
UC	2	Colon	17
UC	3	Ascending colon	17
UC	4	Transverse colon	18
UC	5	Sigmoid colon	7
UC	6	Sigmoid colon	NA
CD	1	Colon	7
CD	2	Ileum	8
CD	3	Ileum	9
CD	4	Ileum	10.5

1111

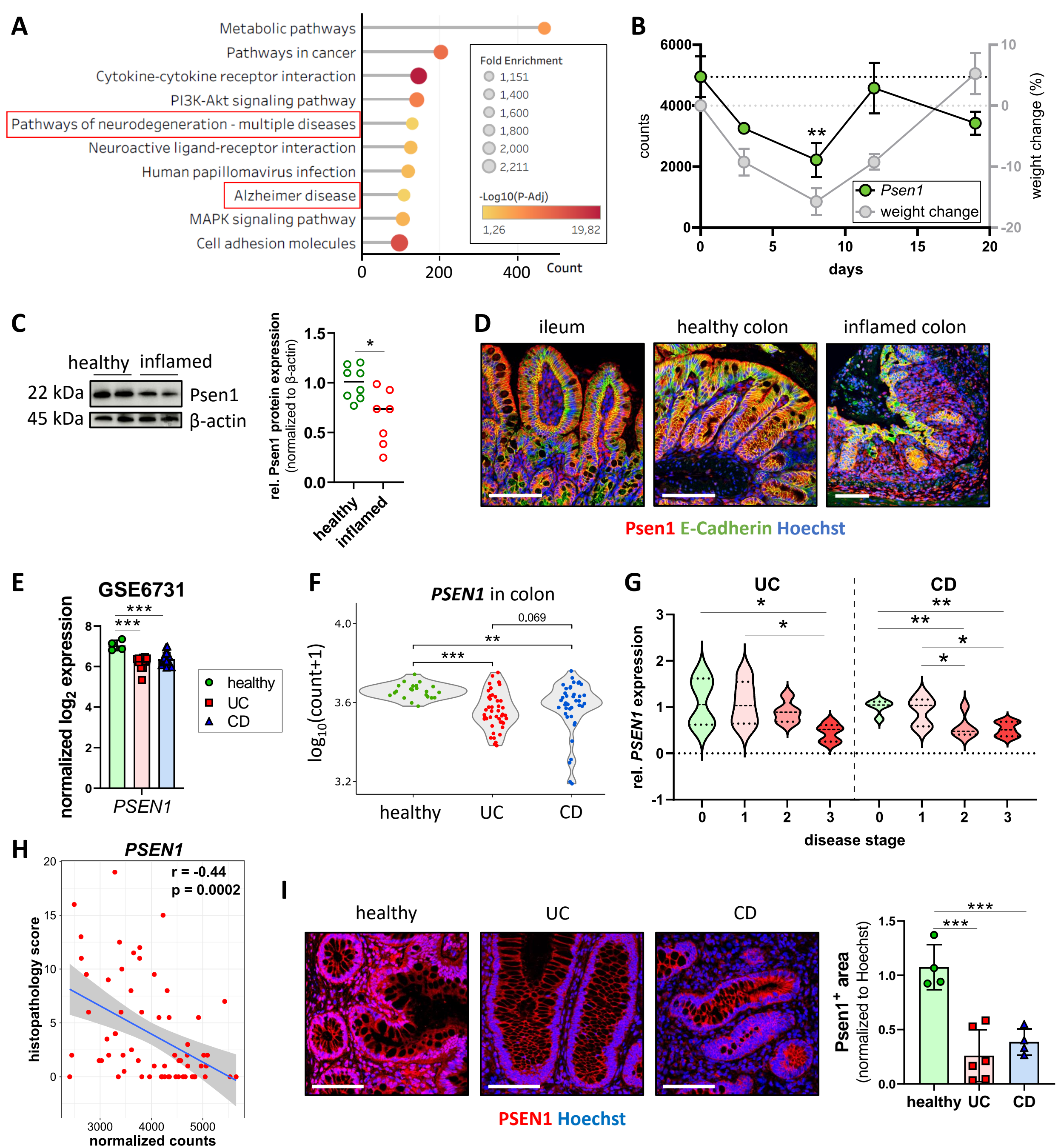


Fig. 1: Psen1 is expressed in the intestine and is differentially regulated during intestinal inflammation

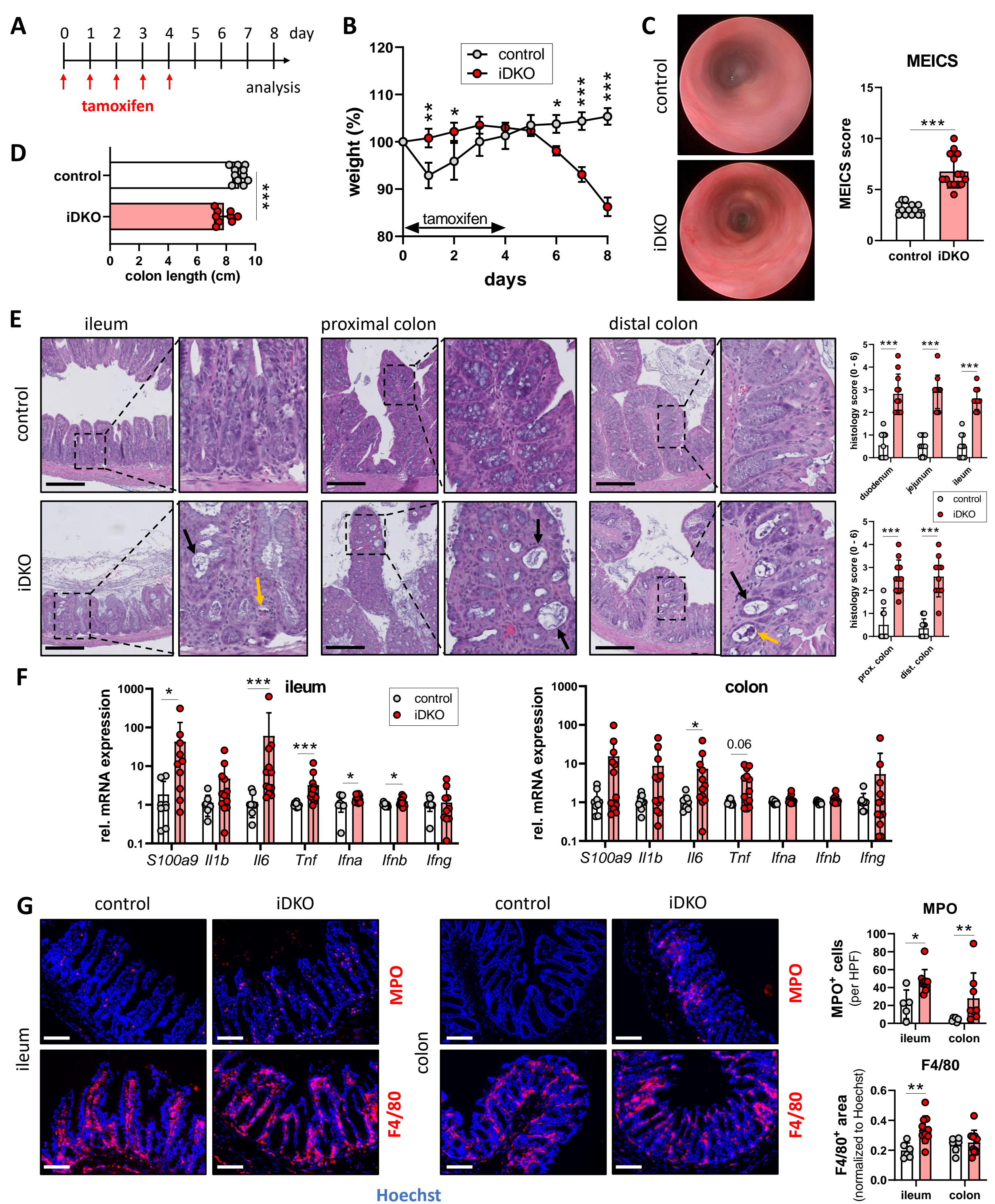


Fig. 2: Inducible *Psen1/2* double knockout mice spontaneously develop colitis

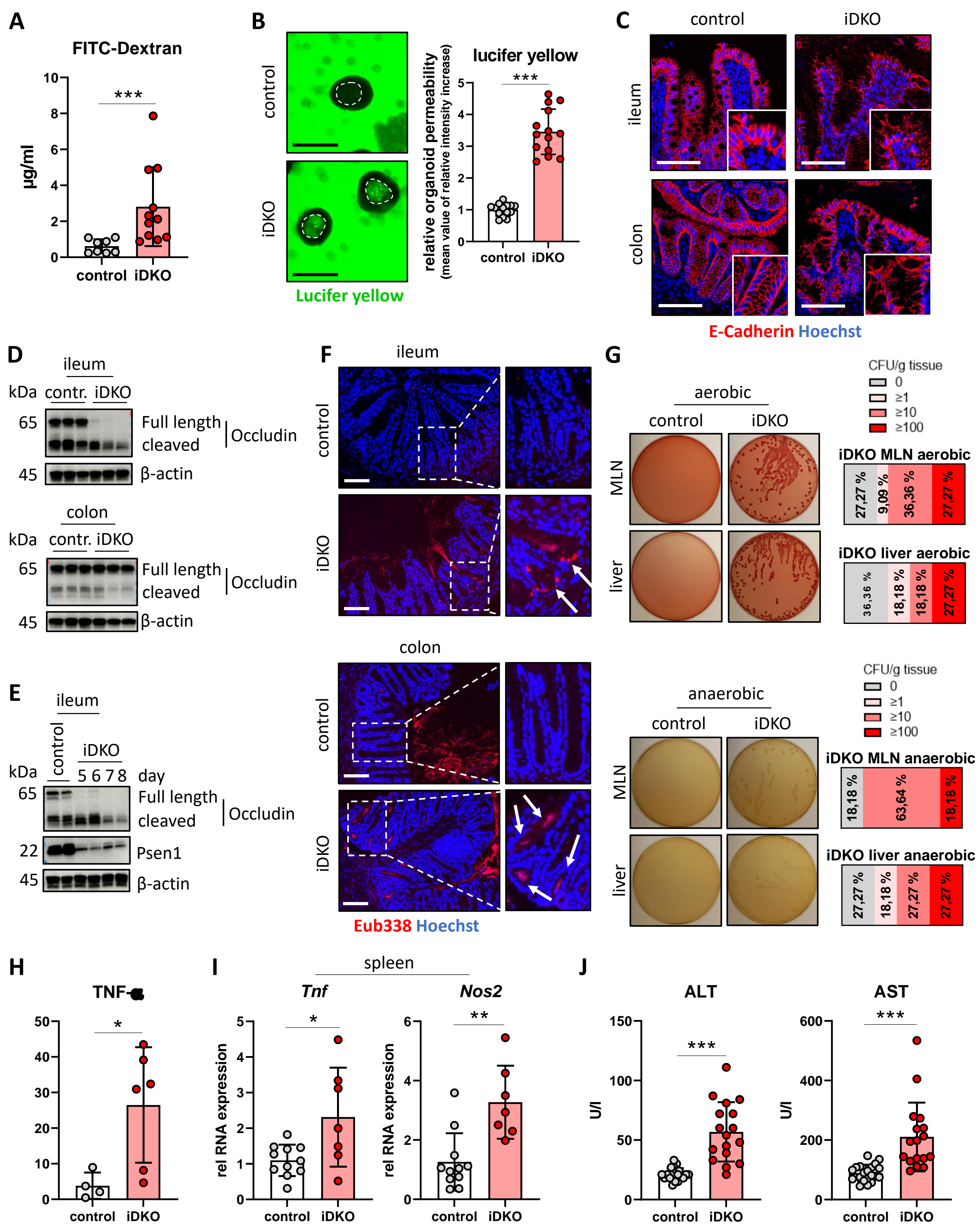


Fig. 3: Presenilins are key to intestinal barrier function

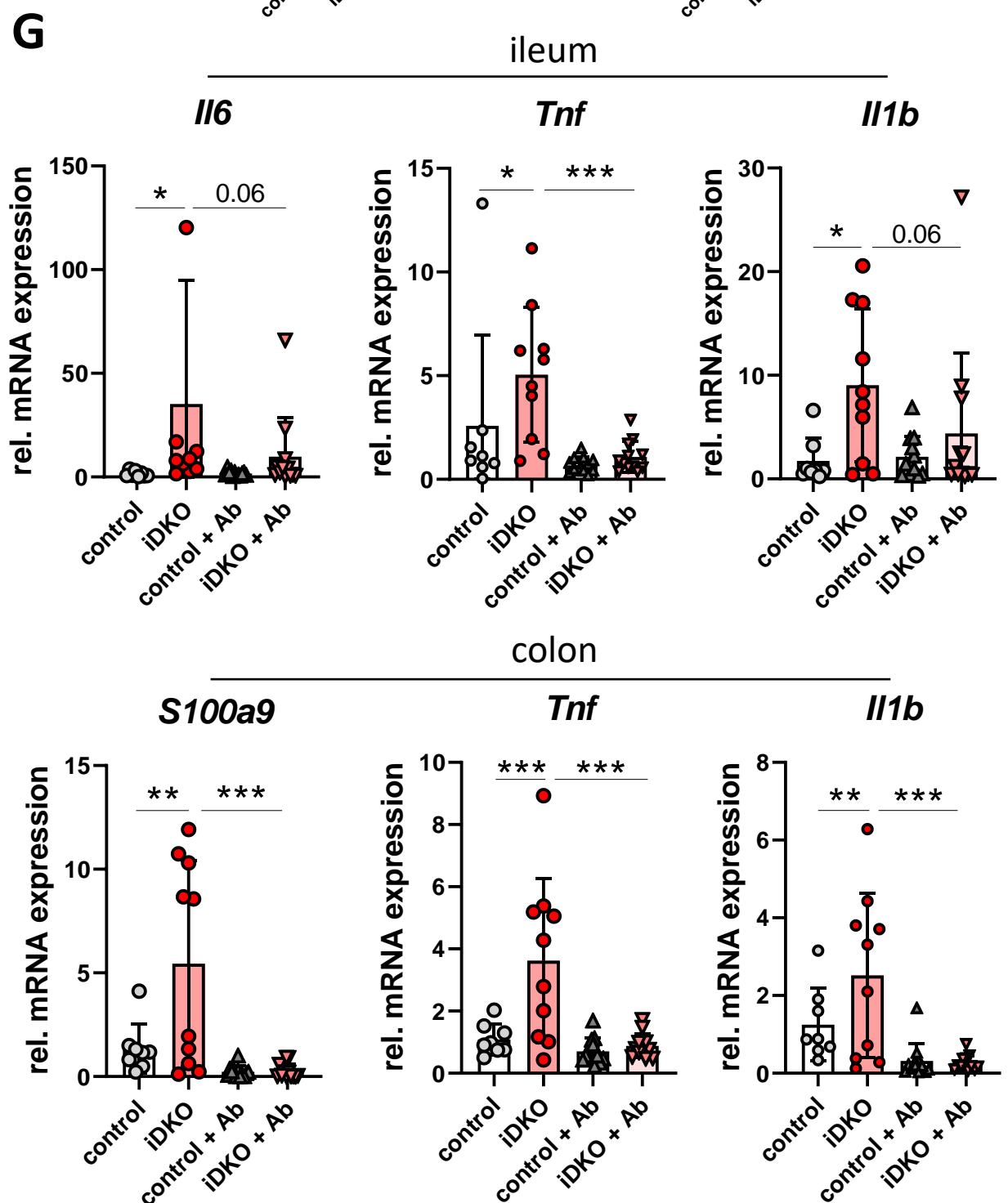
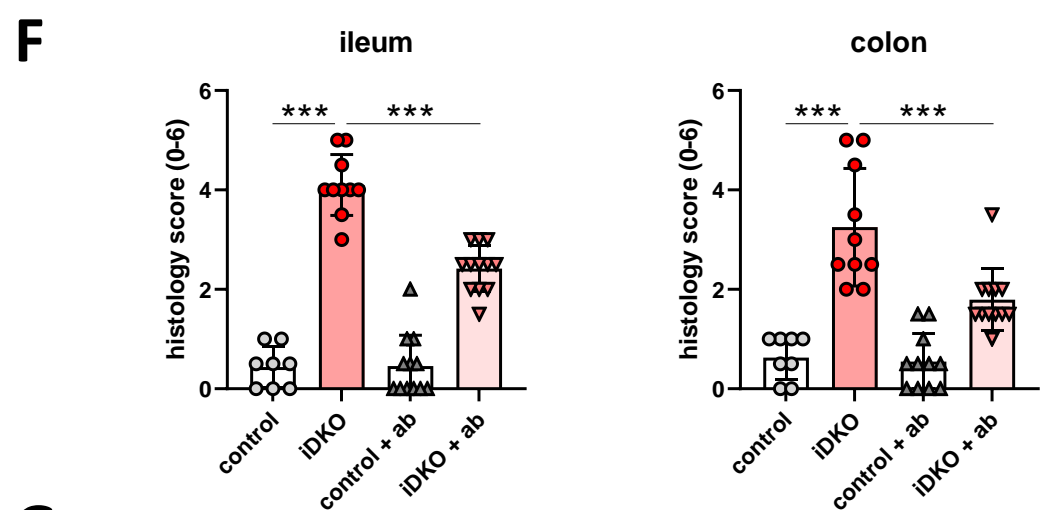
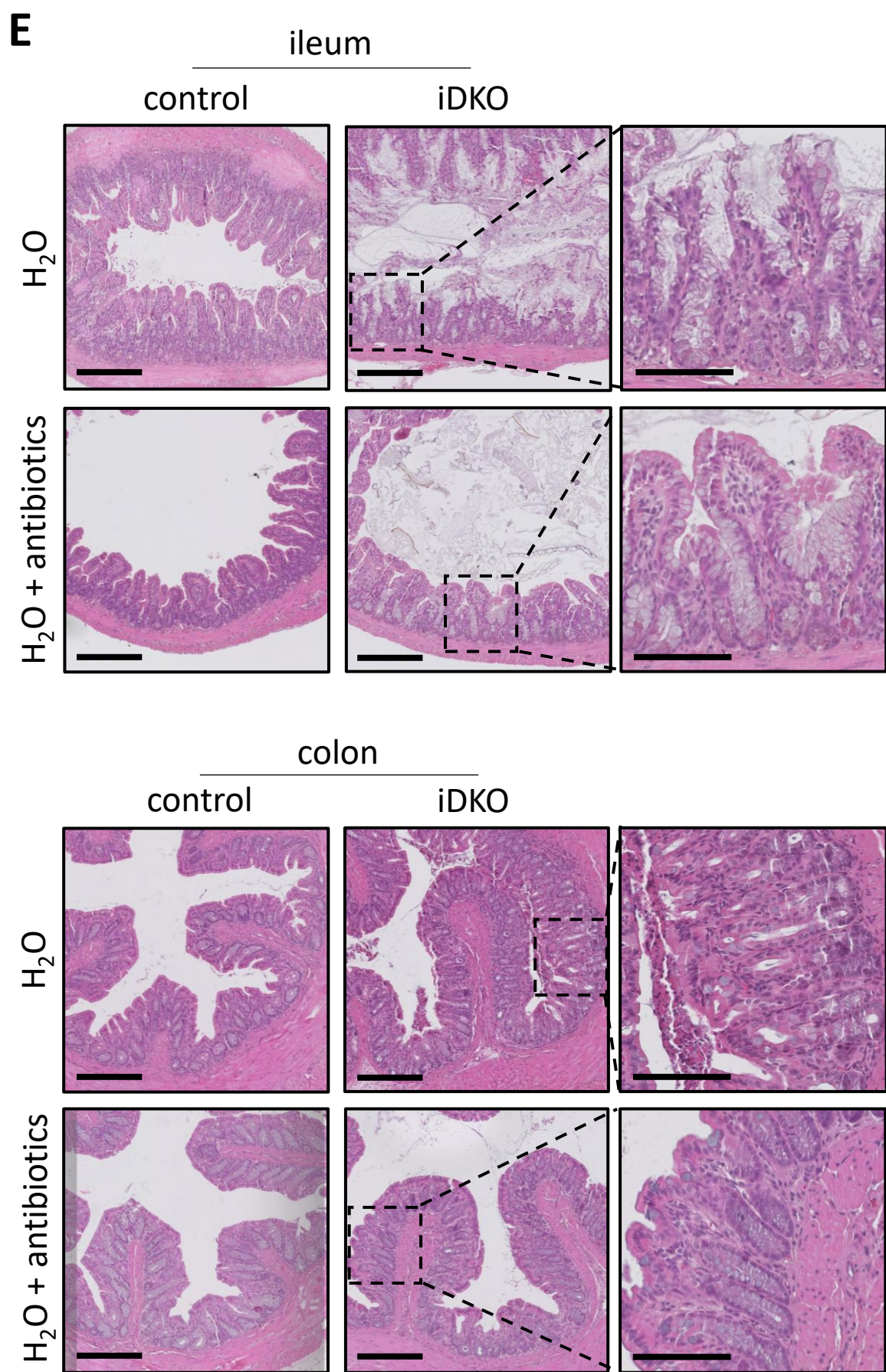
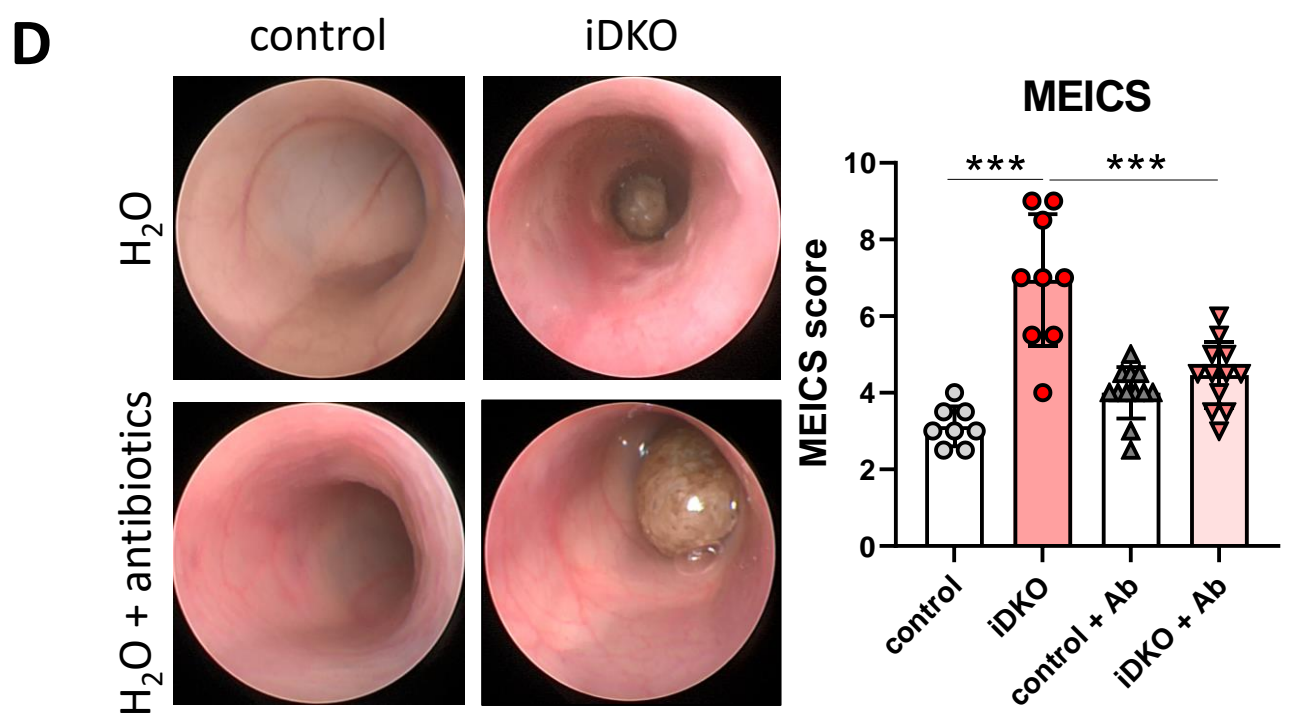
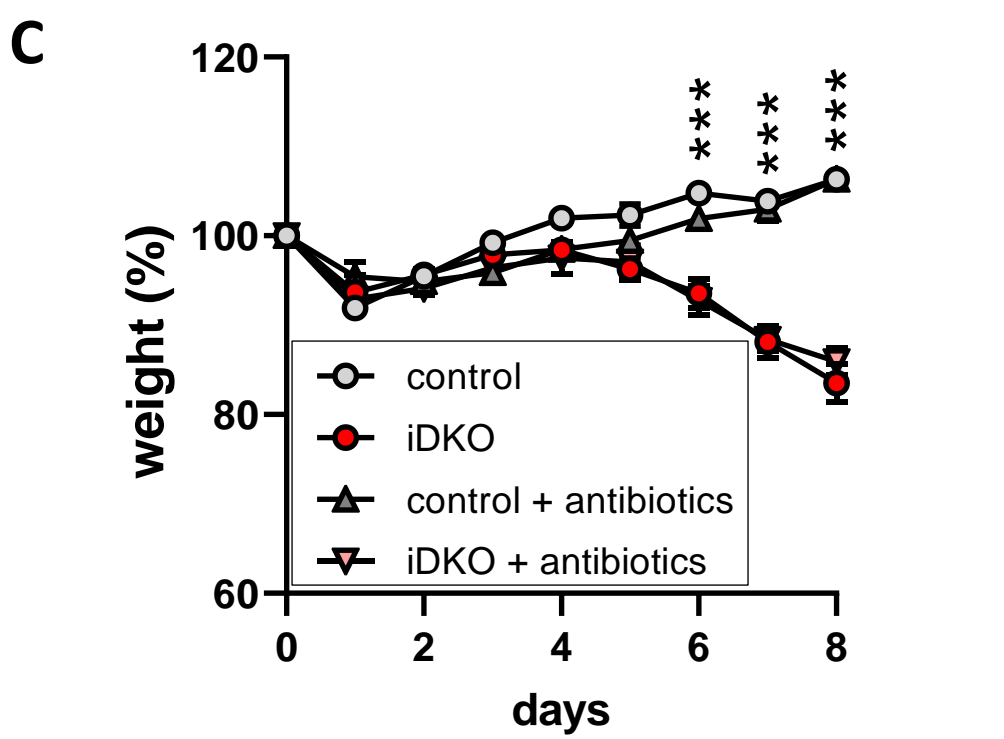
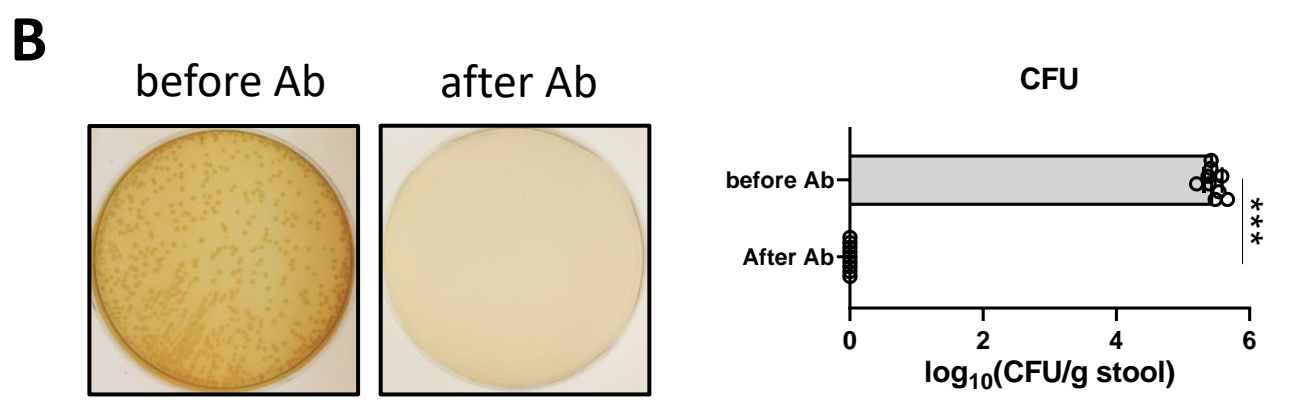
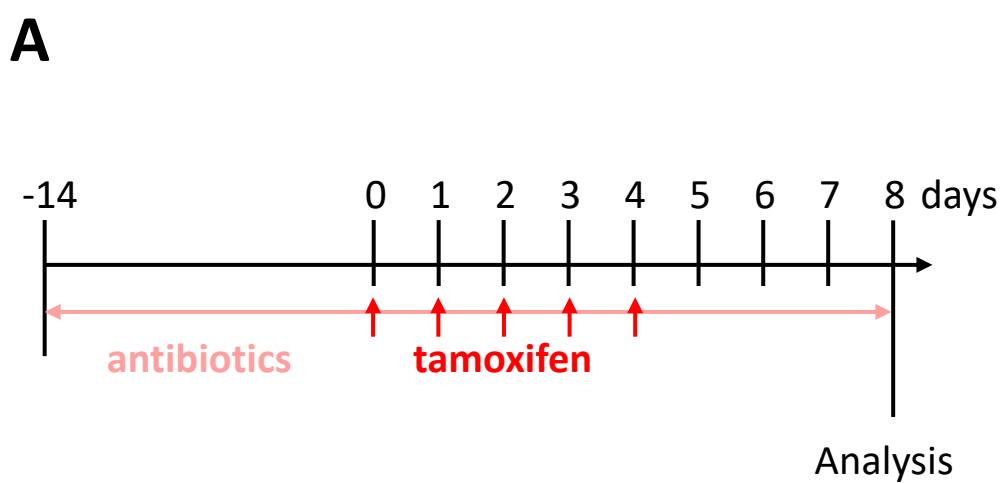


Fig. 4: Microbiota depletion improves spontaneous inflammation but not body weight loss in inducible Psen1/2 double knockout mice

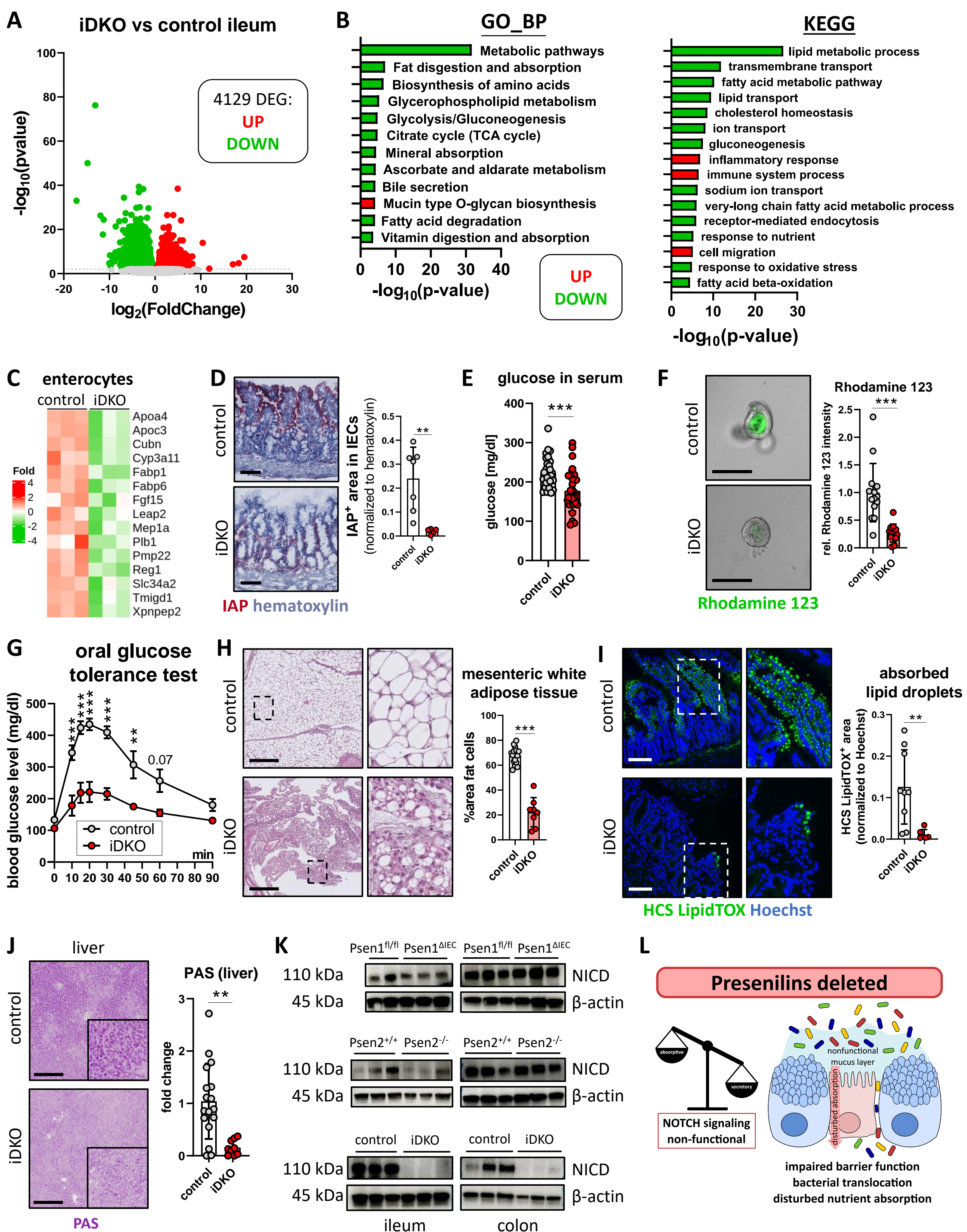
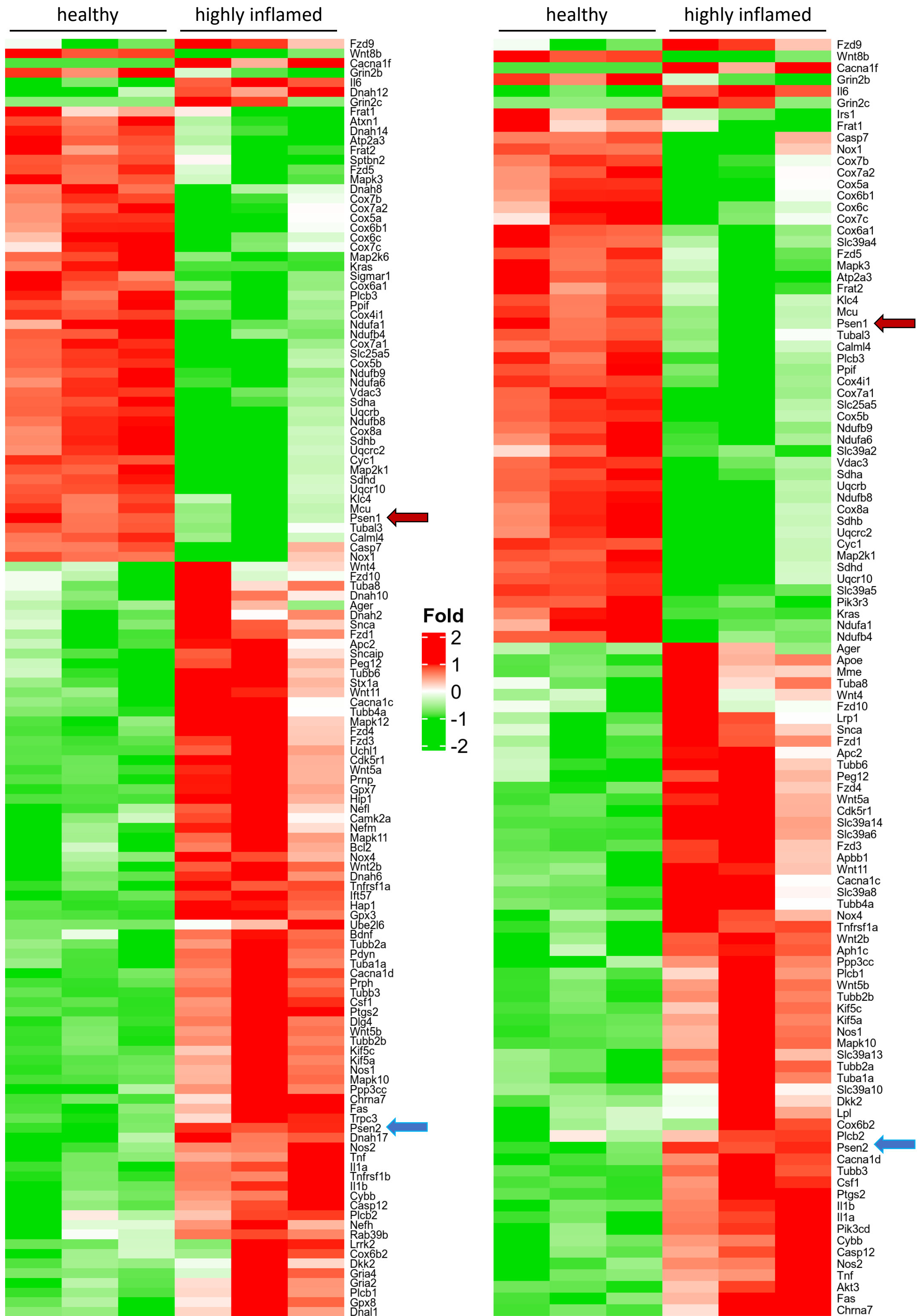


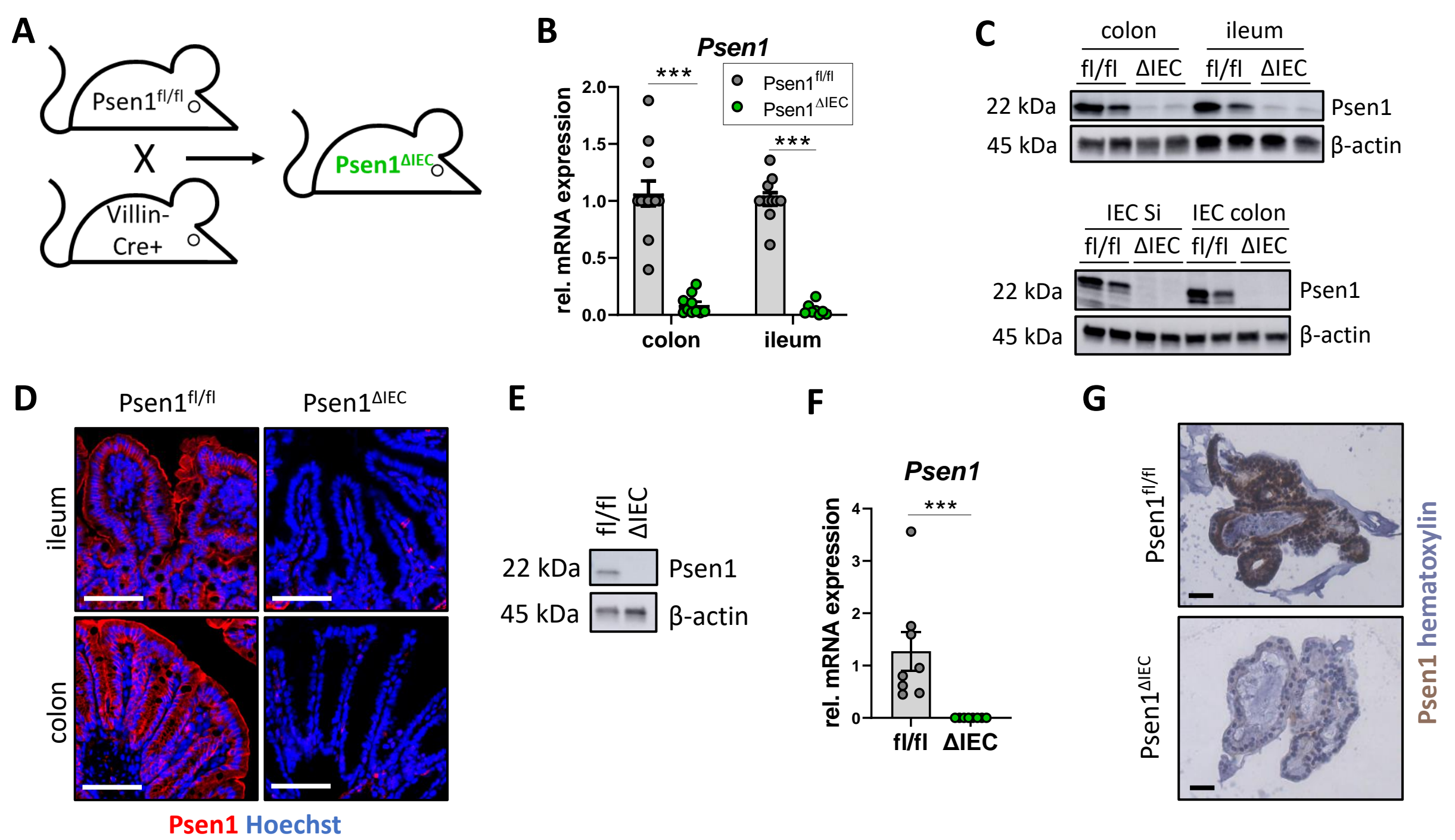
Fig. 5: Dual presenilin deletion leads to enterocyte loss, malnutrition and death in presenilin double knockout mice due to Notch signaling disruption

Pathways of neurodegeneration – multiple diseases

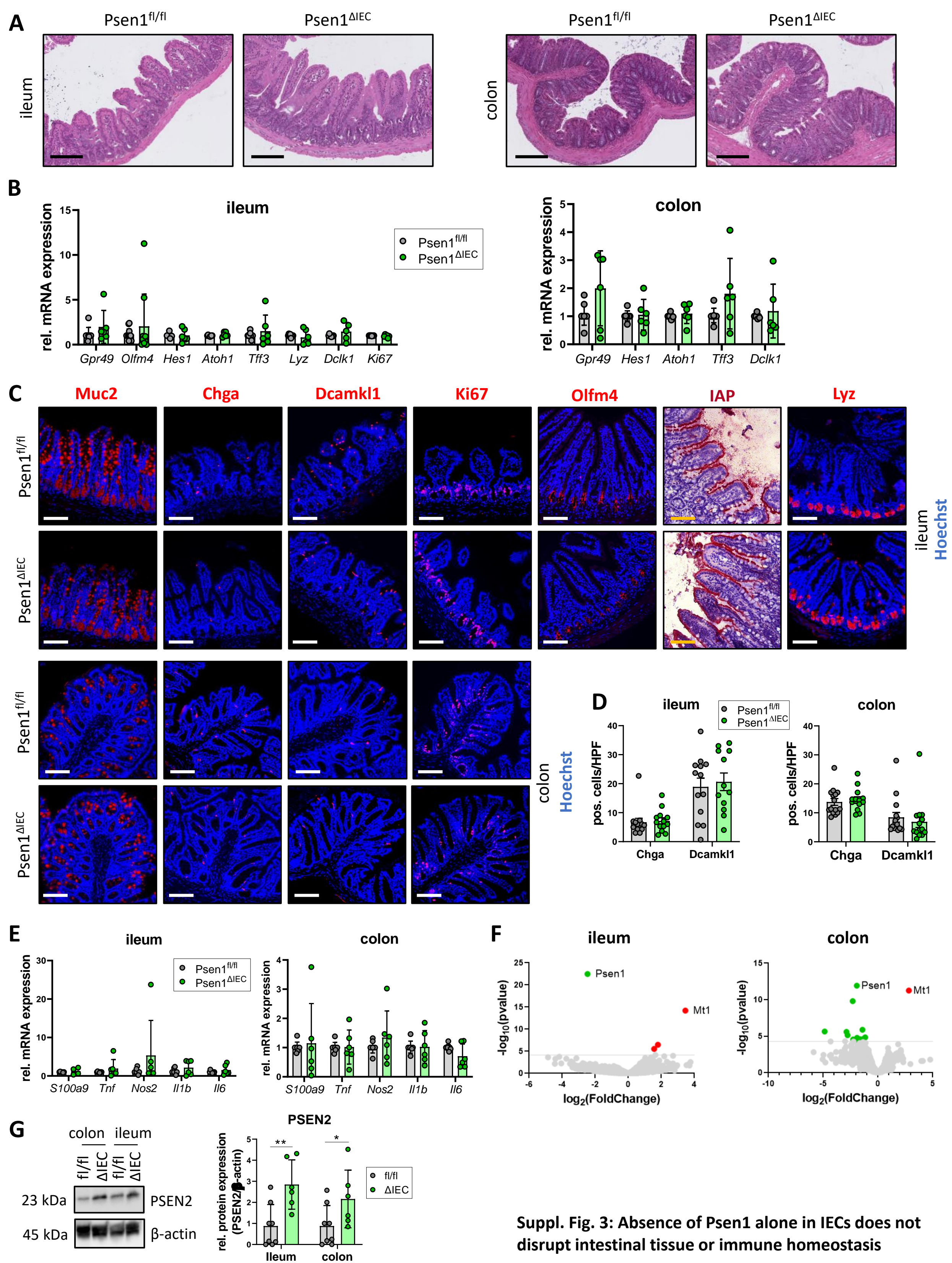
Alzheimer's disease

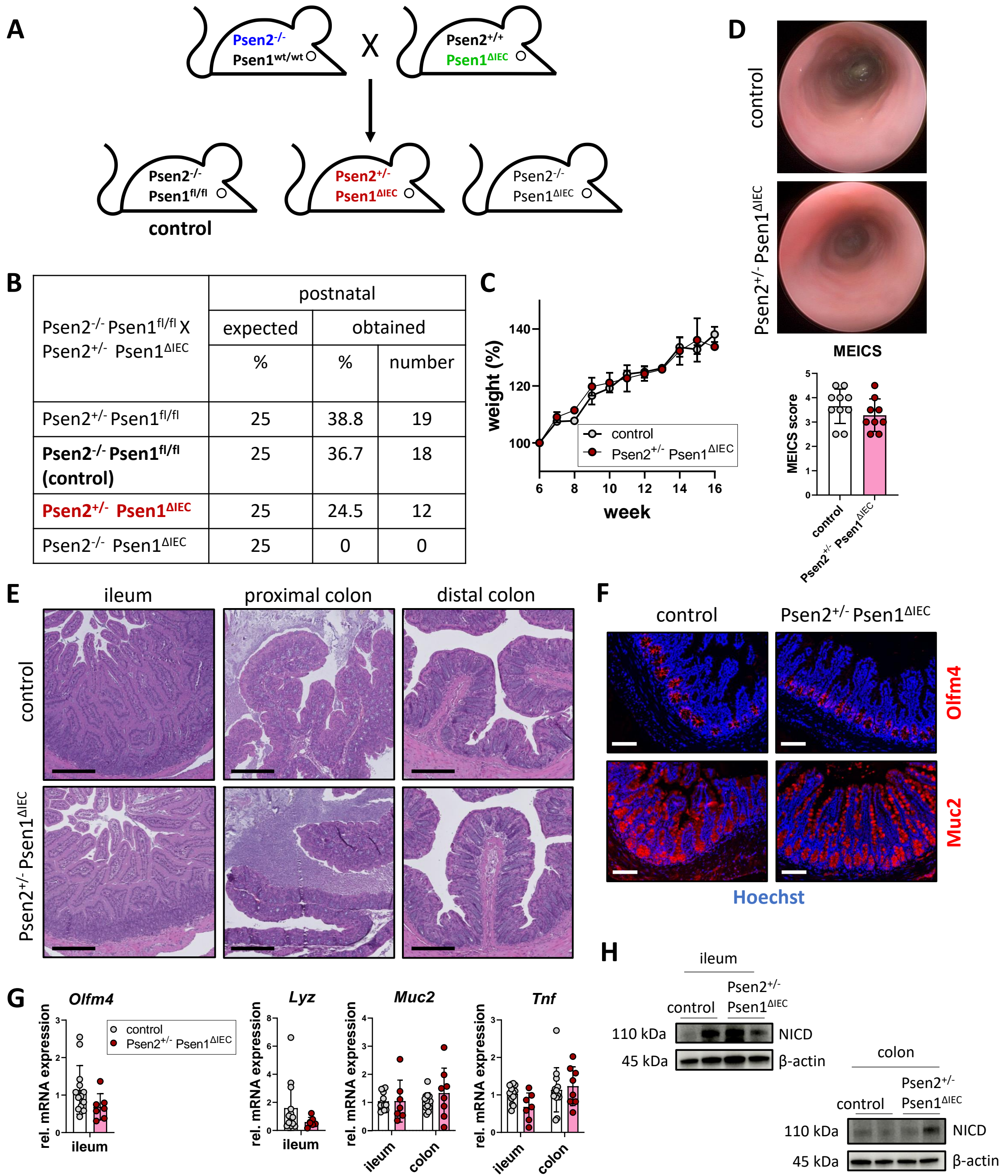


Suppl. Fig. 1: Involvement of genes associated with neurodegeneration and Alzheimer's disease in intestinal inflammation

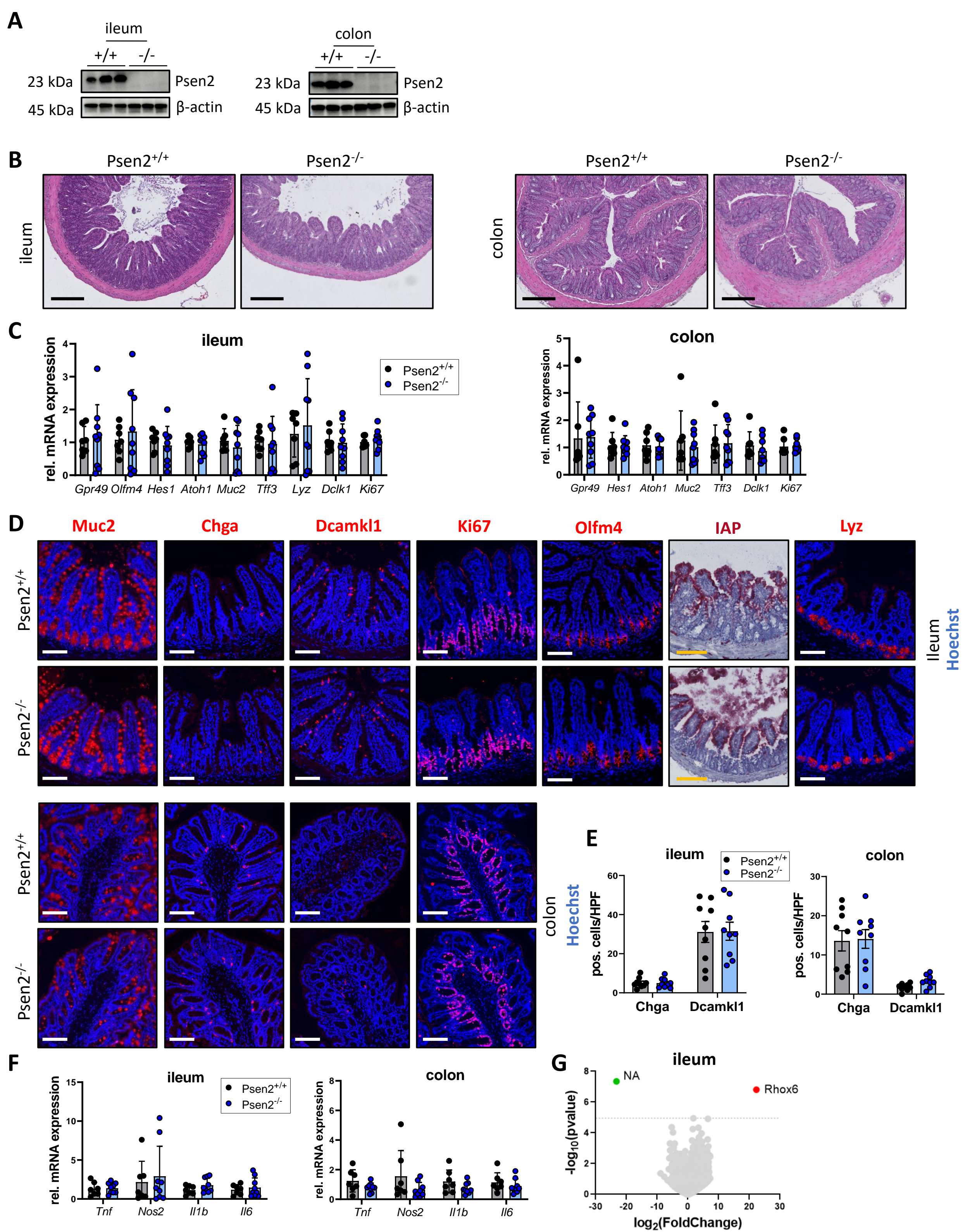


Suppl. Fig. 2: Generation of intestinal epithelial specific *Psen1* deficient mice

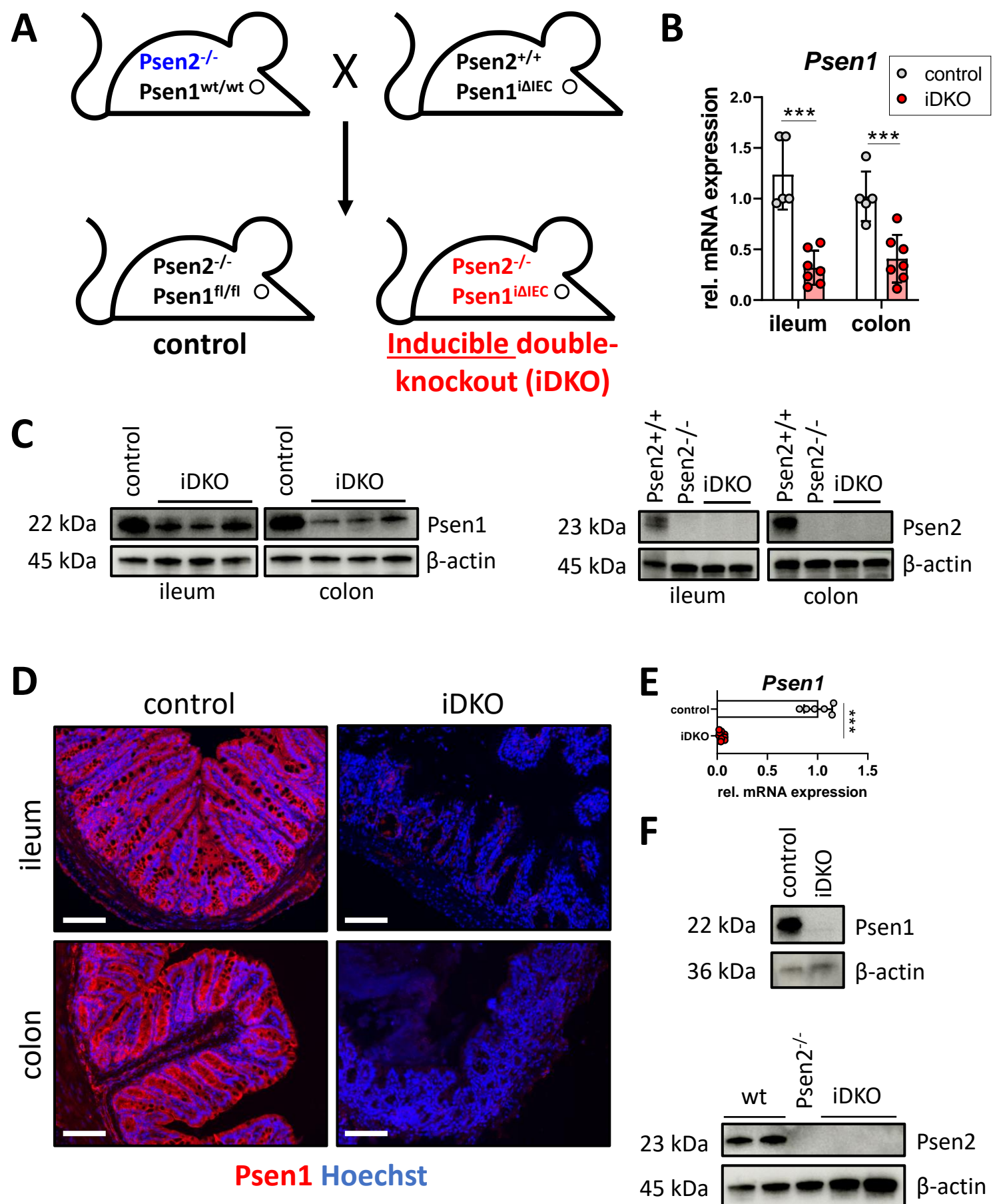




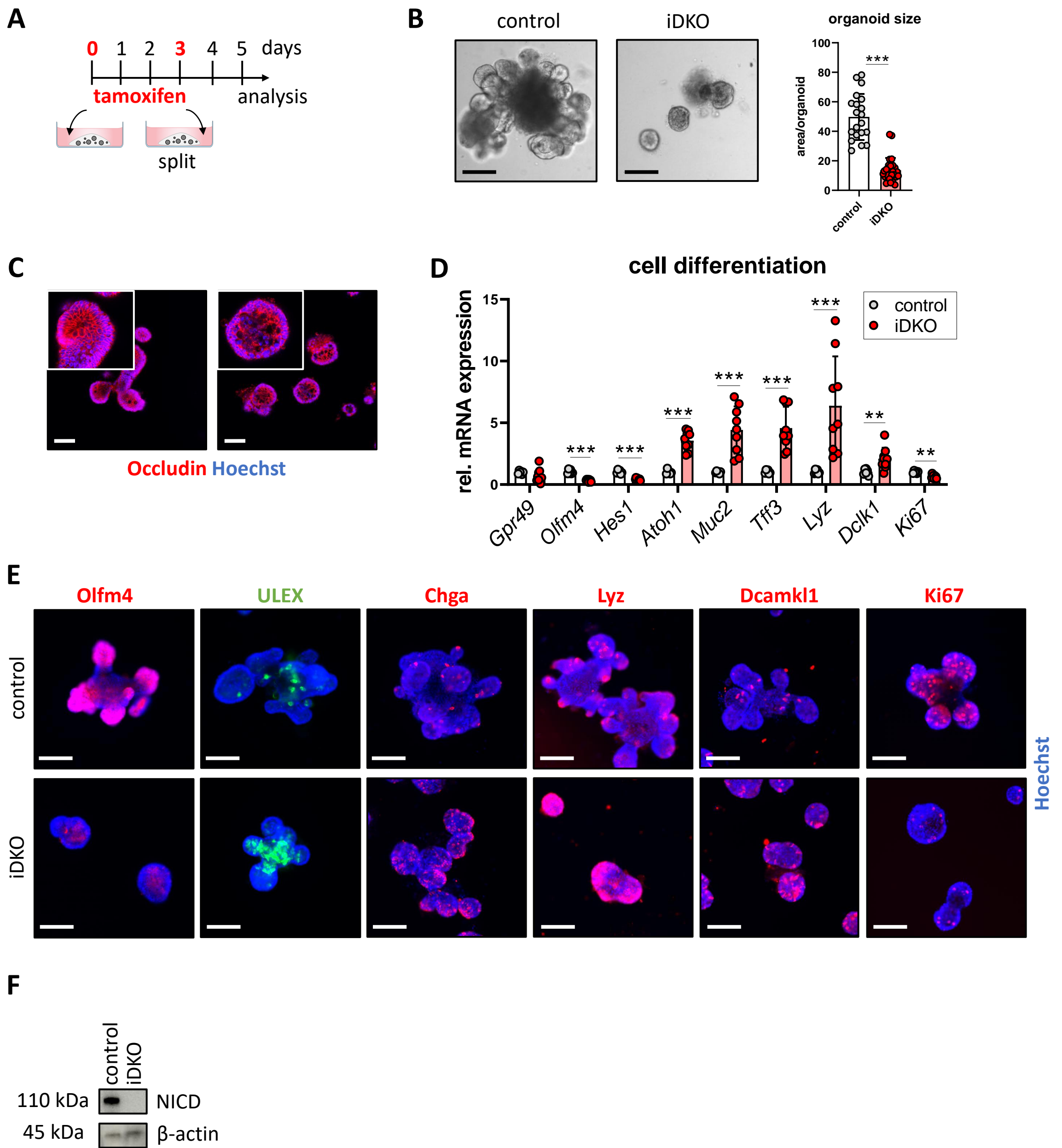
Suppl. Fig. 4: One allele of Psen2 is sufficient to maintain intestinal homeostasis in heterozygous presenilin double knockout mice



Suppl. Fig. 5: Absence of Psen2 alone does not disrupt intestinal tissue or immune homeostasis

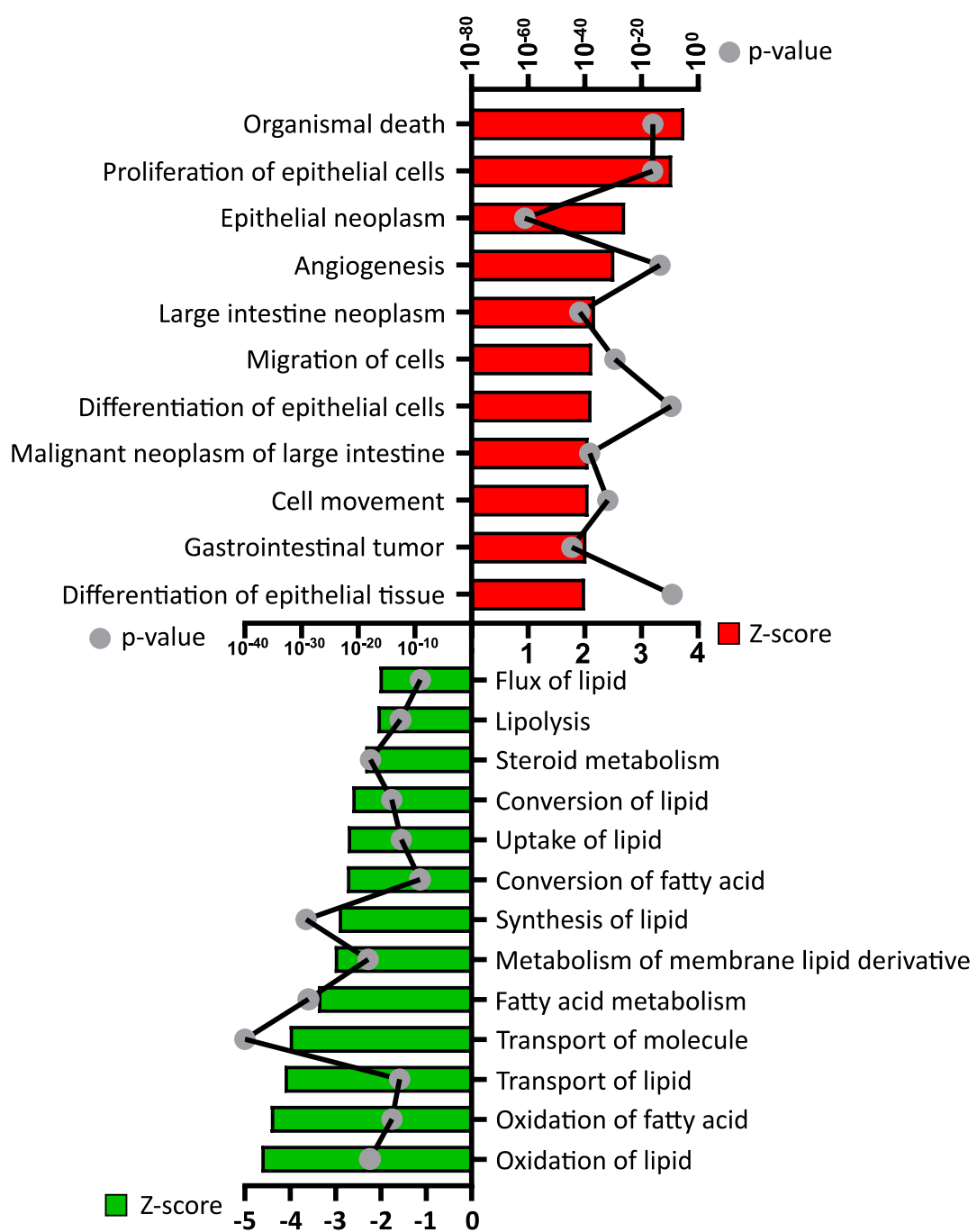


Suppl. Fig. 6: Inducible Psen1/2 double knockout mice lack Psen1 and Psen2 in the IECs

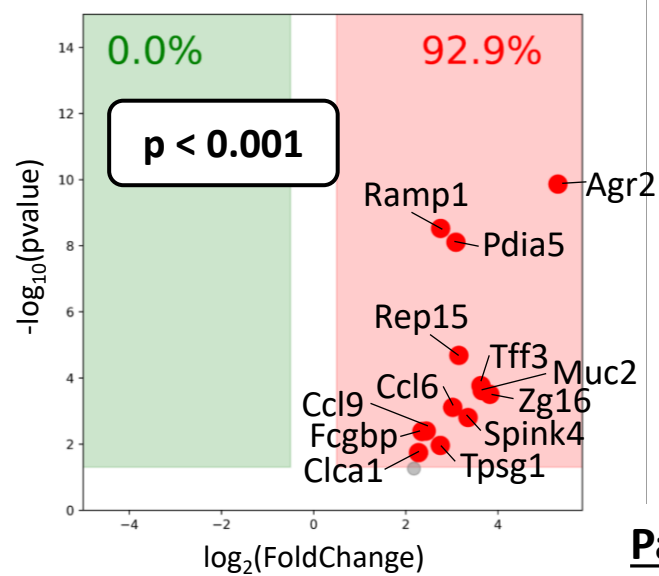


Suppl. Fig. 7: IECs lacking Psen1 and Psen2 have a pro-inflammatory signature and an impaired IEC differentiation

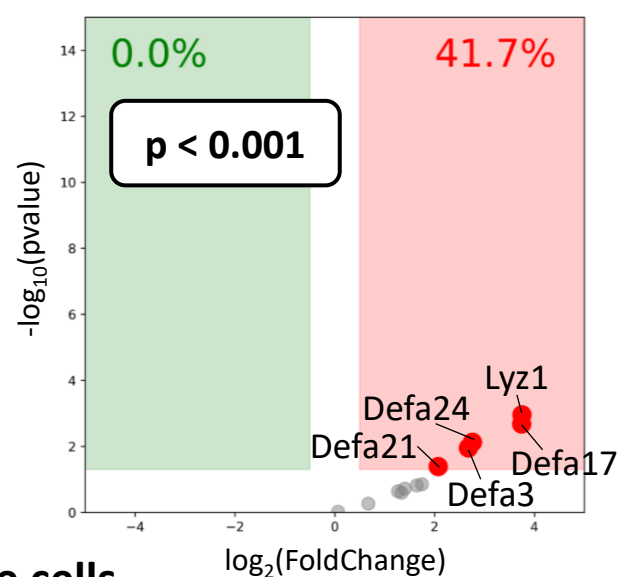
A IPA Diseases and Functions



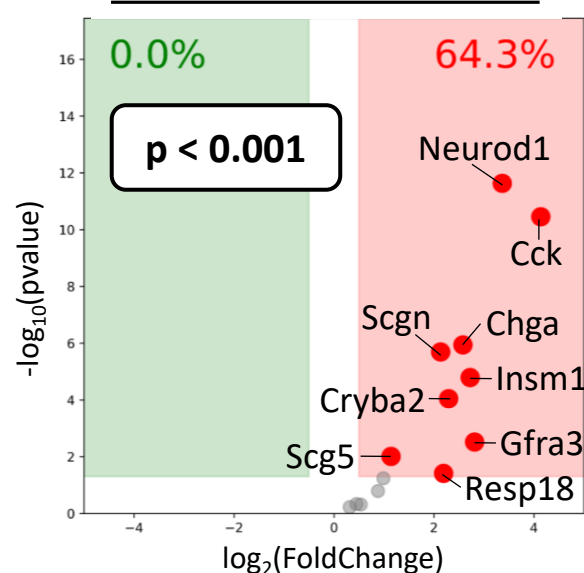
B Goblet cells



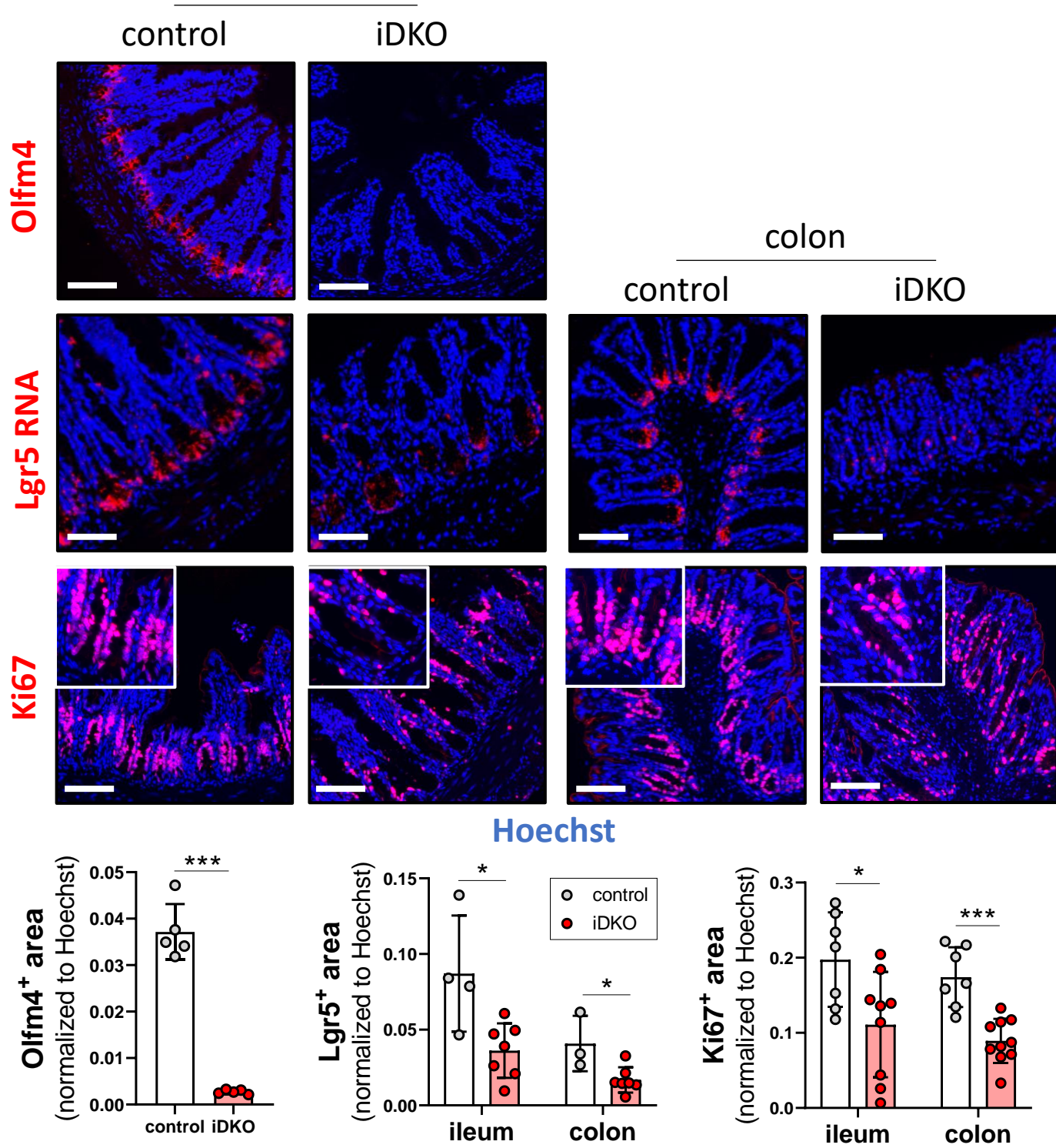
Paneth cells



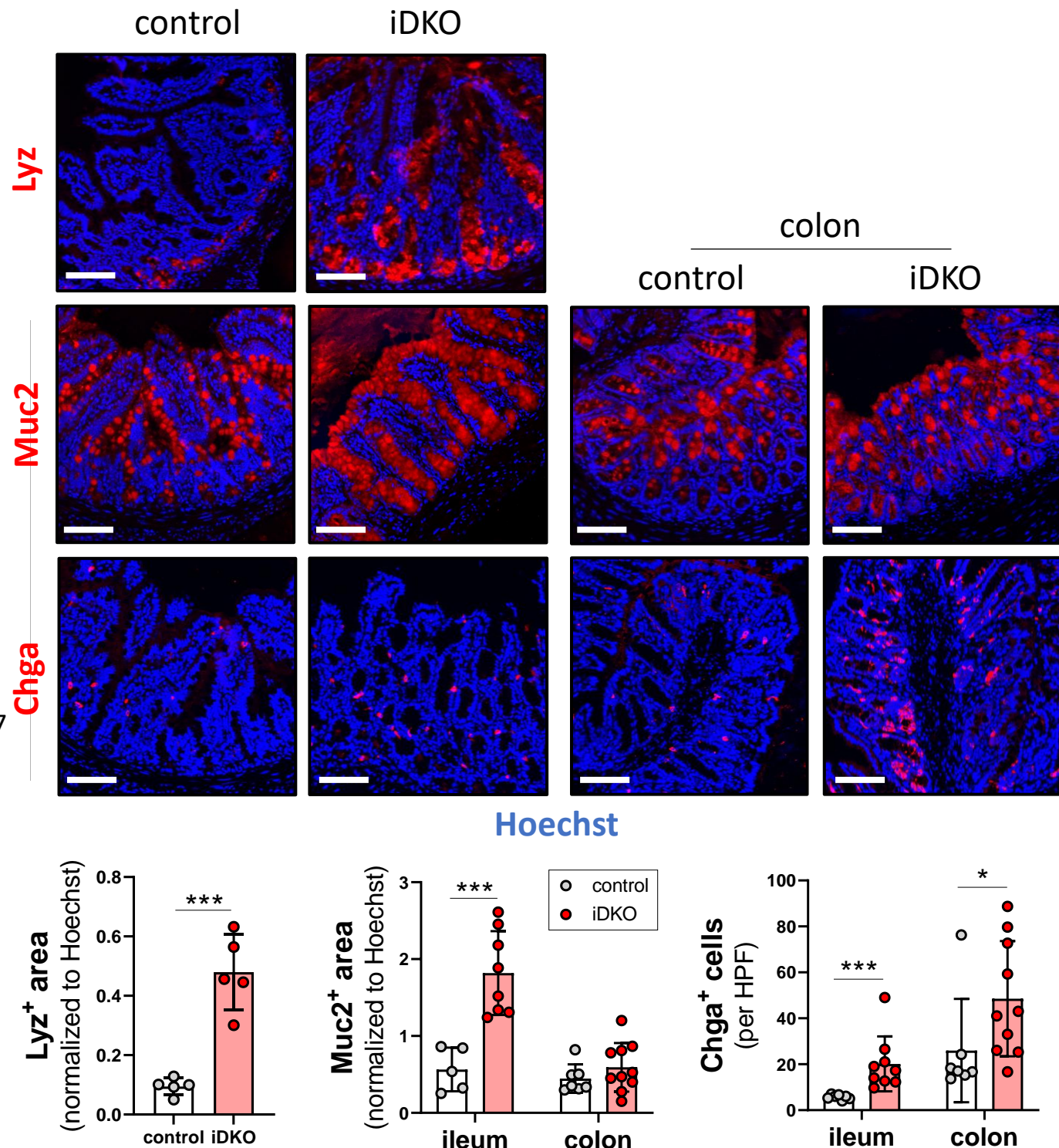
Enteroendocrine cells



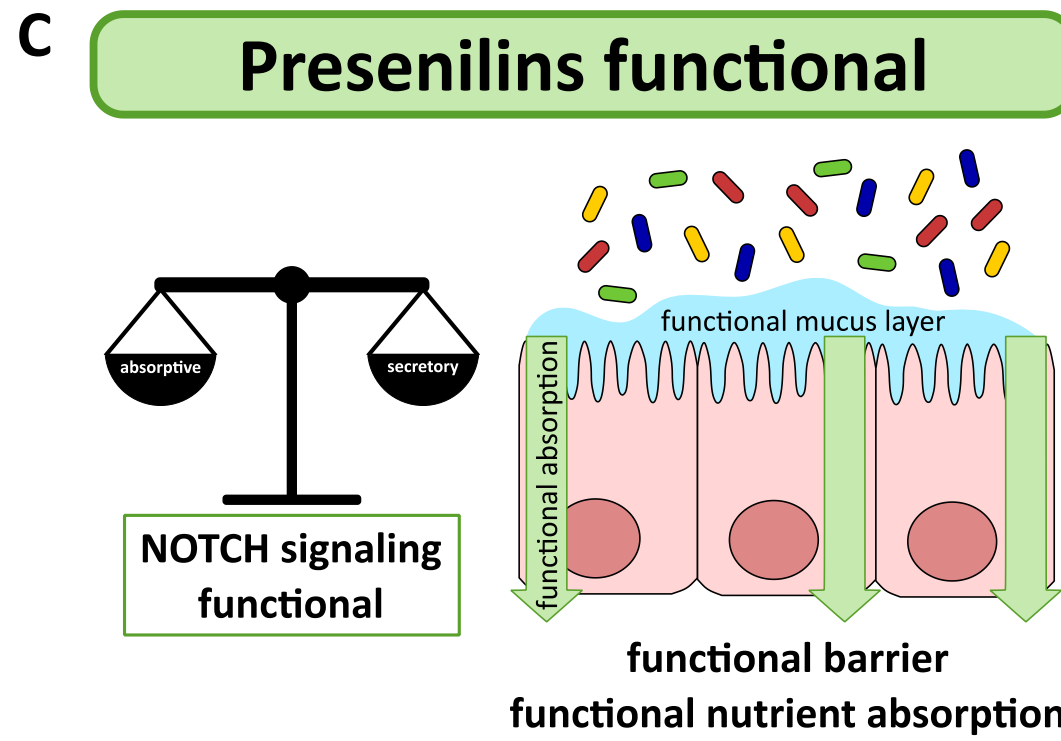
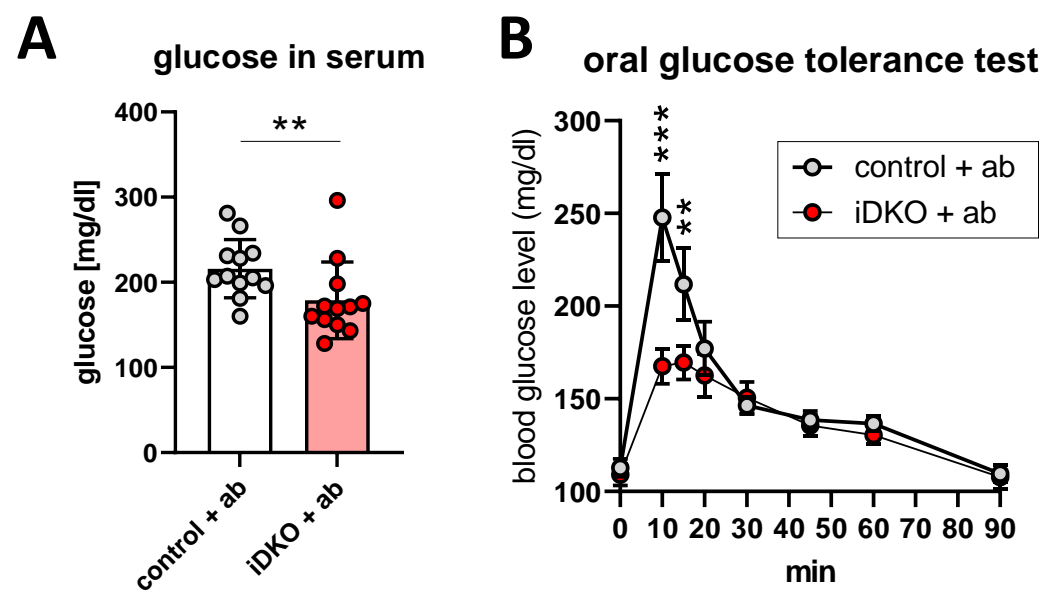
C ileum



D ileum



Suppl. Fig. 8: Psen1 and Psen2 deficiency leads to impaired IEC differentiation



Suppl. Fig. 9: Presenilins play a crucial role in maintaining tissue homeostasis